Developing a Control Strategy for Frequency Stability using Battery Energy Storage System in Microgrid

Thierry Mucunguzi Rwagasore

FACULTY OF ENGINEERING AND SCIENCE

MSc. in Electrical Power Systems and High Voltage, EPSH4-1034

P10 Master Thesis

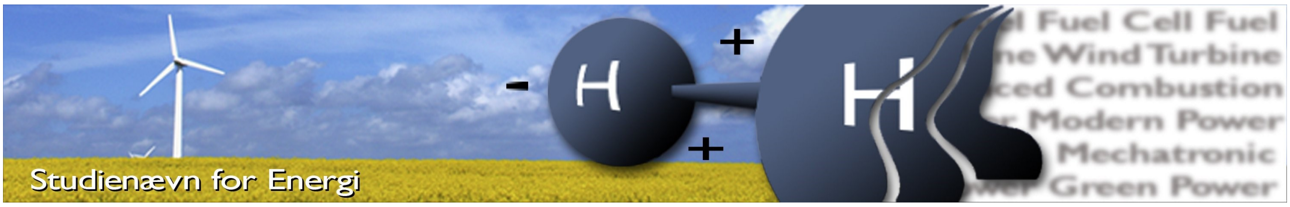

Title:	Developing a Control Strategy for Frequency Stability using Battery Energy Storage System in Microgrid
Semester:	10th. semester
Semester theme:	Master Thesis
Project period:	28.07.2021-28.10.2021
ECTS:	30
Supervisor:	Pavani Ponnaganti
Project group:	EPSH4-1034

Student Name:
Thierry Mucunguzi Rwagasore

Total:	65
Appendix:	8
Supplements:	0

Synopsis

The increase of RESs in the power system creates stability issues such as the frequency rise or fall due to the intermittent nature of RE. To deal with those issues, various advanced technologies have been developed and proposed as the promising solutions, one of those technologies is Battery Energy Storage System (BESS). The main focus in this project is to develop a BESS control strategy for frequency stability in Livø island microgrid containing DERs. This is achieved by carrying out investigations on microgrid, the frequency stability and the BESS technologies. This has led to a development of a BESS control strategy used to provide the primary frequency control into microgrid. The developed BESS control is examined through the performed simulations in DIgSILENT PowerFactory. The simulated results show that the developed BESS control has a positive impact on the frequency stability throughout the examined scenarios. However, it is found out that the BESS size of 5 [kW] power rating is small and cannot store enough power from grid during overproduction, thus through sensitivity analysis, the suitable size of BESS is found to be 25 [kW].

By accepting the request from the fellow student who uploads the study group's project report in Digital Exam System, you confirm that all group members have participated in the project work, and thereby all members are collectively liable for the contents of the report. Furthermore, all group members confirm that the report does not include plagiarism.

Summary

This project aims to develop a control strategy for frequency stability using the BESS. The developed BESS control is used in providing the primary control in the Livø island power system with Distributed energy resources. Initially the background about the modern power systems, storage technologies and the microgrid are introduced in chapter one. In chapter two, it is described the aspect of microgrid operation, Livø microgrid, frequency stability, battery energy storage technologies and the grid code requirements. The chapter three is about the model of the components in microgrid, namely the DG, WT, PV, HWST and BESS. Additionally, the Livø power system network is examined using two critical scenarios in DIgSILENT PowerFactory. In chapter four, it is carried out the implementation of the developed BESS control strategy into Livø power system, and examined through the scenarios described in chapter three. Moreover, the sensibility analysis to find out the suitable BESS size for improving the frequency stability is carried out in chapter five. The discussion on overall project and simulation results is given in chapter six, and conclusion & future work in chapter seven.

Preface

The author of this Master thesis is from Aalborg University (AAU) in Department of Energy Technology. The project focuses on developing a control strategy for stabilizing the system frequency in a microgrid using BESS. The project is written using Overleaf, and the simulations are carried out in DIgSILENT PowerFactory. Furthermore, the graphs and figures are built using the MATLAB and Microsoft Visio.

Readers' Guide

References are specified with the Vancouver method as [number, page]. The bibliography is at the end of the report, where books are denoted "author, title, publisher, edition, year of publication and ISBN". Websites are denoted "author, title, URL, edition, year of publication and last visited in dd/mm/yy", when applicable. Technical reports are denoted "author, title, publisher and year". When referring to figures and tables they are denoted with the number of the chapter and figure/table number. E.g. figure 3 in chapter 2 will be referred to as "Figure 2.3". The figure and table number is written below the given figure and table.

Equations are denoted with the number of the chapter and equation number. E.g. equation 12 in chapter 5, is referenced as "Equation 5.12". The equation number is written on the right hand side of the equation.

Appendixes are found last in the report and listed alphabetically. The appendixes contain the system model in PowerFactory, the description of the component models, settings and consumption profile.

Acknowledgements

The author of this project would like to express a special thanks to his supervisor Assistant professor Pavani Ponnaganti for tremendous help and guidance on completing this project work. I would also like to hank family and friends for their special words of encouragement during my project period.

Nomenclature

Symbols

Symbol	Name	Unit
A	Area	-
C	Capacitance	[F]
E	Energy	[Wh]
f	Frequency	[Hz]
I	Current	[A]
K	Gain	[-]
L	Inductance	[H]
m	mass	[Kg]
P	Active Power	[W]
Q	Reactive Power	[Var]
R	Resistance	[Ω]
S	Apparent Power	[VA]
T	Temperature	[$^\circ$ C]
t	time	[s]
V	Voltage	[V]
ρ	Air density	[Kg/m^3]
ω	Angular frequency	[rad $\cdot s^{-1}$]
1,2,3,4,5,...	Index numbering	[-]

Subscripts

Symbol	Name
1,2,3,4,5...	index numbering
d	direct
e	electrical
f	feedback
i	internal

L	load
m	mechanical
max	maximum
min	minimum
nom	nominal
pv	photovoltaic
q	quadrature
ref	Reference
srnd	Surrounding
STD	Standard

Abbreviations

Abbreviation	**Definition**
AC	Alternating Current
AVR	Automatic Voltage Regulator
B	Bus
BESS	Battery Energy Storage System
BMS	Battery Management System
CHP	Combined Heat Pump
CO_2	Carbon dioxide
DC	Direct Current
DER	Distributed energy resource
DG	Diesel generator
DSO	Distribution system operator
DTU	Danmarks Tekniske Universitet
El-boiler	Electric boiler
ES	Energy Storage
ESS	Energy Storage System
FSM	Frequency Sensitive Mode
HP	Heat Pump
HWST	Hot Water Storage Tank
IEEE	Institute of Electrical and Electronics Engineers
IGBT	Insulated Gate Bipolar Transistor
LFSM-O	Limited Frequency Sensitive Mode-Over frequency

LFSM-U	Limited Frequency Sensitive Mode-Under frequency
Li-Ion	Lithium Ion
LV	Low Voltage
MPPT	Maximum power point
PCC	Point Common Coupling
PCS	Power Conversion System
PI	Proportional Integral
PLL	Phase-Locked Loop
POC	Point of Connection
p.u.	Per Unit
PV	Photovoltaic
PWM	Pulse Width Modulation
RES	Renewable Energy Source
RMS	Root Mean Square
SG	Synchronous Generator
SOC	State of Charge
SWP	Solid Wind Power
TV	Television
VRFB	Vanadium Redox Flow Battery
VSC	Voltage Source Converter
VSG	Virtual Synchronous Generator
WT	Wind Turbine

Table of Contents

Chapter 1 Introduction **1**

1.1 Background 1

1.2 Microgrid 3

1.3 Green Livø 4

1.4 Problem statement 4

1.5 Structure of the project 5

1.6 Delimitations 5

Chapter 2 State of the art **6**

2.1 The aspect of microgrid operation 6

2.2 Livø Microgrid 7

2.3 Frequency stability 8

2.4 Battery energy storage technologies 10

2.4.1 Lead-Acid Batteries 11

2.4.2 Lithium-Ion batteries 12

2.4.3 Vanadium Redox Flow Battery (VRFB) 12

2.4.4 Sodium-Sulfur Batteries 12

2.4.5 The battery and power management 14

2.5 The grid code requirements 14

Chapter 3 Modelling of the components in Microgrid **16**

3.1 Diesel Generator (DG) 16

3.1.1 Governor 17

3.1.2 AVR 18

3.2 Wind turbine 19

3.3 PV 20

3.4 Hot water storage tank 21

3.5 BESS model 22

3.5.1 Battery 22

3.5.2 Converter 23

3.5.3 BESS controller 23

3.6 BESS control strategy 24

3.7 Livø power system network 26

3.7.1 1st scenario: Low consumption and High RE 30

3.7.2 2nd scenario: High consumption and Low RE 32

Chapter 4 Implementation of the BESS control strategy in the system model 34

4.1 1st scenario: Low consumption and High RE 34

4.2 2nd scenario: High consumption and Low RE 36

Chapter 5 Sizing of BESS for improving the frequency stability 40

5.1 1st Scenario: Low consumption and high RE 40

5.2 2nd Scenario: High consumption and low RE 42

Chapter 6 Discussion 44

6.1 System operation before BESS sizing 44

6.2 System operation after BESS sizing 45

Chapter 7 Conclusions 46

Bibliography 47

Appendix A System model in PowerFactory 49

A.1 BESS model 49

A.2 PV model 52

Appendix B Actual load profile 55

1 | Introduction

This chapter aims to introduce about the background of the project, microgrid and green Livø. In addition, the problem statement, structure of the project and delimitations are provided.

1.1 Background

In the modern power systems, the renewable energy sources (RESs) such as wind turbines (WTs) and photovoltaics (PVs) are increasingly integrated and contributing with a high capacity of electric energy in power grid. It can be emphasized by the danish energy consumption status, where the electricity consumption from RESs has exceeded 50 % of the total consumption in 2020, and this is expected to increase to 100 % by 2030 [1]. The continuous growth of the RESs is aiming to reduce the conventional generation based on the fossil-fuel due to the concern of climate changes, and also to meet the increasing energy demand resulted from population and industrial growth. However, the increase of these RE technologies in the power system creates the imbalance between the supply and demand, and thereby the frequency deviation due to their intermittent nature. In addition, the inability to provide various control options for frequency stability which are normally provided by the conventional synchronous generators such as the inertia reserve to the utility grid. The inertia plays a major role in preventing the sudden changes which may arise in system frequency by storing or releasing the kinetic energy in rotating masses of synchronous generators. However the RESs like WT generators are connected through conversion system interfaces to utility grid, and this isolates the kinetic energy of the WT generators from grid during frequency changes [2].

To mitigate these frequency stability issues, the energy storage (ES) technologies combined together with a control strategy are among the promising solutions in future power systems with highly penetration of Renewable energy technologies. The energy storage will help to handle the fluctuated generation from RES, and will also need a control system in order to optimize the balance between the supply and demand. The energy storage system (ESS) can have different definitions depending on its application, however in this case it can be defined as a technology device interfaced to the grid to store the surplus electric power by charging during overproduction, and then the stored electric power is later delivered back by discharging during power deficit. The ES technologies are classified into different categories based on their working principle as shown in figure 1.1. The characteristics of each type of ES technology can be describe as following [3]:

- **Pumped storage hydropower**: is a mechanical energy storage device with the ability to store the largest amount of energy capacity by this time. The working principle of this device is based on two reservoirs of water placed on different height levels. The energy is stored by pumping the water from lower reservoir to the upper reservoir using the surplus electric power. On the hand, the power generation happens when the water falls from the top to lower reservoir.
- **Compressed air-energy storage**: This type of storage device performs its task using the gas turbine. It stores the energy through compressing the air into the chamber using the surplus power. Then the electricity is generated by releasing the air through the turbine during the power deficit.
- **Flywheels**: The flywheel devices perform the storage task through motor-generator compound. This converts the energy into rotational inertia during overproduction, and this is later extracted to provide the power during overload.
- **Battery energy storage**: This device consists of electrochemical cells through which the electrical energy is stored in form of chemical reactions using the surplus power, and this is later converted back to electricity during power deficit.
- **Thermal energy storage**: This device stores the electrical energy in form of heat from the surplus electric power. The stored heat can either be used to provide heating or converter back to electric power.
- **Super-capacitors**: These store the electrical energy in form of electrostatic charge. These devices provide high fast response to the power demand, but can only supply less amount power compared to most other storage technologies.
- **Hydrogen storage**: The energy is stored in chemical reaction, where the hydrogen can be obtained from water through electrolysis process and the surplus electrical power.

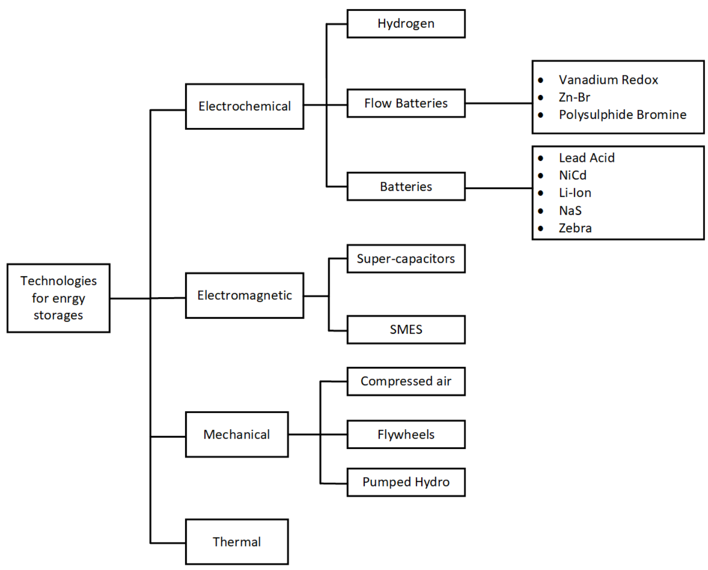

Figure 1.1: Classification of energy storage technologies

The Battery Energy Storage System (BESS) has various benefits over other ES technologies like its cost efficient, safety and its flexibility as it can be installed in any location without restrictions, unlike the pumped hydro storage and compressed air energy storage that require huge water tank and underground air reservoirs. Therefore, the BESS is to be considered in this project and will be used to provide the frequency stability in the system with varying power from RES. The optimization of utilizing various distributed generation units such as WTs, PVs, micro-turbine, BESS technologies into the future power grid has initiated the microgrid concept. The interest in microgrid has increased due to various reasons as described in Section 1.2.

1.2 Microgrid

Microgrid can be defined as a self-sufficient power system composed by distributed generations, ESS and loads. Despite of its capability of operating independently, the microgrid is usually connected to the main grid, unless it is placed in remote areas where there is no utility grid. The figure 1.2 shows an overview of microgrid structure. It can be seen that it is composed by Distributed generation such as WTs, PVs, combined heat and power unit (CHP), microturbines; distributed energy storages (DESs) such as battery banks, super-capacitors, flywheels, electric vehicle; flexible loads and control devices [4].

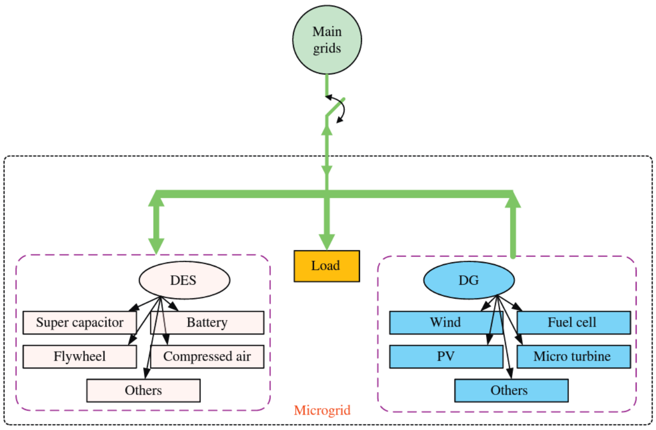

Figure 1.2: A typical structure of a Microgrid[4]

The microgrid with high integration of RES may face the stability issues due to the intermittent power generation from RESs, therefore, it is usually connected to main grid to keep it more reliable and stable. However, the microgrid may provide a number of advantages and some are listed below:

- Facilitate the integration of RESs, and thereby reducing the usage of fossil fuels
- Increase the quality of the supplied power due to decentralisation, better balance between demand and generation etc.
- Provide highly reliable power to a wide range of customers, both residentials and commercials.

- Useful to rural areas with no access to the utility grid, and also to the areas facing large power outage.

In this project, the microgrid to be investigated will be based on the Livø power system which is powered by the Diesel generators (DGs), WT and PV. Moreover, the flexible loads such as heat pump (HP) and electric boiler are integrated in the system.

1.3 Green Livø

Livø is a danish and nature conservation island of 320 hectare shown in Figure 1.3, that is located in Limfjord. This island is managed by the Danish Nature Agency and is used as a touristic area where it is open for tourism services during summer and receives around 20,000 guests each year.
In accordance with Denmark's goal of converting to 100 % renewable energy supply by 2050, it is initiated a Green Livø project in 2012 by the Danish Nature Agency aiming to convert the Livø power system into a self-sufficient system with fossil-free energy sources. Therefore, from 2015 to 2019 the Energinet has initiated the first stage of restructuring the Livø power system, by installing the RE sources namely the PV and WT, the bio-diesel generators, and also the flexible loads to support the power balance such as heat pump, electric boiler, oil boiler, wooden boiler, BESS and hot water storage tank (HWST) [5].

Figure 1.3: Livø island [6]

1.4 Problem statement

The main focus of this project is to investigate and develop a BESS control strategy for frequency stability in the microgrid containing RES. This is achieved by carrying out investigation on the following points:

- Microgrid and its operating principle
- Power management into the Livø power system

- Frequency stability
- BESS technologies
- Danish grid codes
- Used components of the considered system network

1.5 Structure of the project

This project consists of 7 chapters as indicated in Figure 1.4. The first chapter contains the project background, microgrid concept, green livø, problem statement and delimitations. The second chapter includes the aspect of microgrid operation, Livø micorgrid, Frequency stability, battery energy storage technologies and grid code requirements. The third chapter is about the modelling of the system components, proposed BESS control strategy and Livø power system network. The fourth chapter is about the implementation of the BESS control strategy in the system model. The fifth chapter is about sizing of BESS for improving the frequency stability, the sixth chapter is about discussion and seventh gives the conclusion & future work.

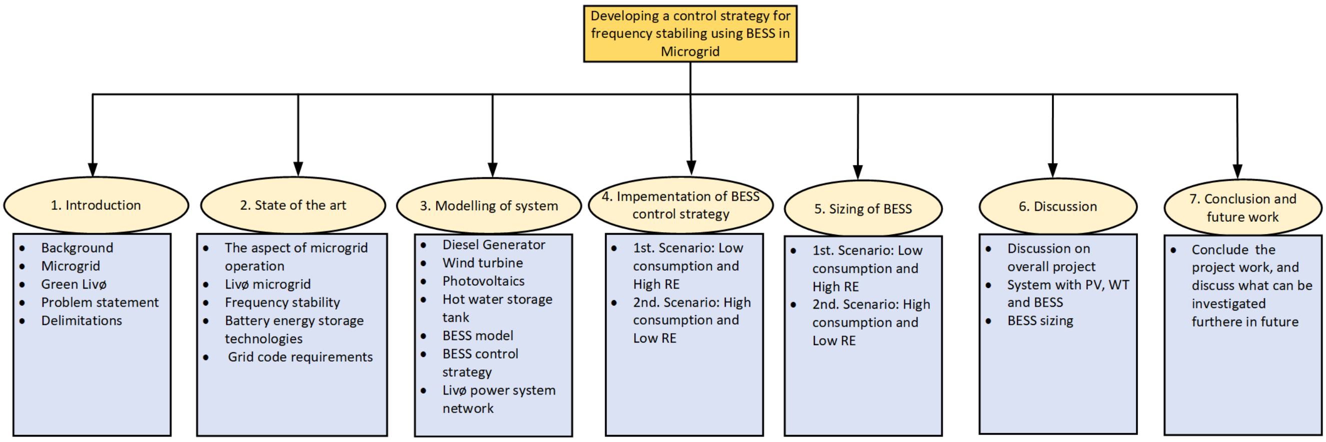

Figure 1.4: Overview of the project structure

1.6 Delimitations

All the aspects related to the project topic are not covered in this project, it is therefore important to list the considered limitations as following:

- Voltage & angle stability are not investigated in this project
- The component models are the standard models in DIgSILENT PowerFactory
- The Battery is modelled as a voltage source
- El-boiler is modelled as constant power load
- WT is modelled as constant power source
- Heat management part is not taken into account

2 | State of the art

This chapter is going to cover some of the important points such as: The aspect of microgrid operation, Livø microgrid, Frequency stability, Battery energy storage technologies and Grid code requirements.

2.1 The aspect of microgrid operation

As previously described, a microgrid has the ability to accommodate various distributed generation units such as microturbines, WTs and PVs. The microgrid may be connected to main grid through a point of common coupling (PCC), where it can serve as power source to the most critical loads of the main grid during fault occurrence. Moreover, a microgrid can also operate independently by supplying the power to an isolated community or rural areas with no access to the main grid. The insufficient of inertia from the distributed generators in a microgrid may result to stability challenges like unstable frequency especially in an islanded microgrid. To have an overview of a modern power grid also know as smart grid and a conventional grid, their differences are gathered in the Table 2.1. The control of

Table 2.1: Comparison between conventional grid and smart grid [7].

Conventional grid	Smart grid
Electromechanical	Digital
One-way communication	Two way communication
Centralized generation	Distributed generation
Few sensors	Sensors throughout
Manual monitoring	Self monitoring
Manual restoration	Self-healing
Failure and blackouts	Adaptive and islanding
Limited control	Pervasive control
Few customer choices	Many customer choices

a microgrid depends on its operation mode. During the grid-connected operation mode, the microgrid may operate as either a controllable load or power source depending on the difference in power ΔP ($\Delta P = P_{Load} - P_{Gen)}$. If $\Delta P > 0$, the microgrid will operate as the load to the main grid, however when $\Delta P < 0$, it is an indication of the surplus power on the microgrid side, therefore the microgrid will deliver the power to the main grid. On the other hand if $\Delta P = 0$, it is an indication of the balance between the power generation and demand, thus no power exchange will occur between the main grid and microgrid. In addition, there are sensitive and nonsensitive-load feeders in a grid-connected microgrid. The sensitive-load feeders must be maintained ON all the time, since they supply power to the sensitive loads, however the nonsensitive-load feeders may be shut down when fault occurs in the main grid.

In case of islanded operation mode, the microgrid is disconnected from the main grid, and the DERs, BESS and other generation units operate independently, where they are controlled individually. In this case, the microgrid must ensure the balance between the supply and demand, the acceptable power quality, voltage & frequency stability and communication among the microgrid components [7].

Now the basic understanding about a microgrid and its operating principle is given, thus it is needed to get overview on the microgrid operation at Livø island that is to be examined further in this project.

2.2 Livø Microgrid

The considered power system in this project is based on Livø island that is powered by the Diesel generator (DG), WT and PV. The increase in WT and PV supply in system causes the reduction of DG supply as well as the DG's control reserves, and this may create stability issues in the system. Thus, the BESS and other devices like el-boiler and HP are integrated in the system to support the stability in the system. In this case, to maximize the usage of WT and PV while maintaining the system stable and reliable, a proper power system structure is needed by modifying the generation and consumption pattern. It can be emphasized that only the management of the power in the system will be considered, however the heat management will not be investigated. As it can be seen in the flow chart of the power management shown in Figure 2.1, the generated power from DG, WT and PV is utilized with respect to the defined conditions described in that flowchart. In this case, the DG have a dual operation aspects in the system, the first one is that it must always operate with a minimum load to ensure the stability and reliability in the system, and the second aspect is that the DG must operate only when the power demand is not covered by the WT and PV. The PV and WT generation is variable since they depend on the sunlight and wind, however during their production, the generated power flows directly to the power consumers. During overproduction, a part of surplus power is stored in BESS and the rest is used by HP and el-boiler to generate the heat. Then, the stored power in BESS is delivered to the grid during peak-demand.

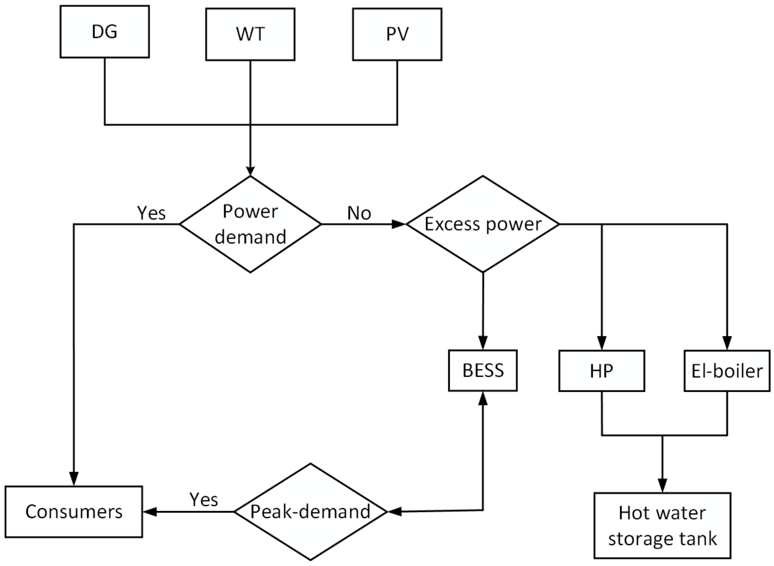

Figure 2.1: Overview on the power management strategy in the system

Since the frequency is one of major factors for power quality in the system, therefore it must always remain within the defined operational range to ensure the stability in the system.
In the next section, the frequency stability and the used control methods are described.

2.3 Frequency stability

The frequency is needed to be maintained nearly constant to ensure the stability and reliability in a power grid. This is achieved by maintaining the active power balanced in the system using different control reserves, where some are inherent in the synchronous machine, and others are provided by the central control centre. The common frequency control methods are described as below:

- **Inertial control reserve**: This type of control reserve is inherently provided by the synchronous machine using the kinetic energy that is stored in the rotating masses of machine, that is later released when the frequency deviates from the nominal value.
- **Primary control reserve**: This control reserve is automatically executed by a speed governor that senses the speed change of generator due to change in load, and then adjust the output power of generator. The basic configuration diagram of speed governor connected together with turbine and generator can be seen in Figure 2.2.

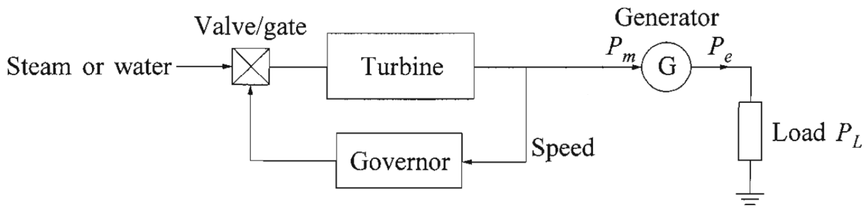

Figure 2.2: Diagram of speed governor with generator [8]

P_m denotes mechanical power, P_e is the electrical power and P_L is the load power.
The frequency deviation from the nominal value due to changes occurring in load (P_L) causes the imbalance between P_m and P_e, which automatically affects the turbine speed. The governor control with droop characteristics responding to the change in speed is illustrated in Figure 2.3.

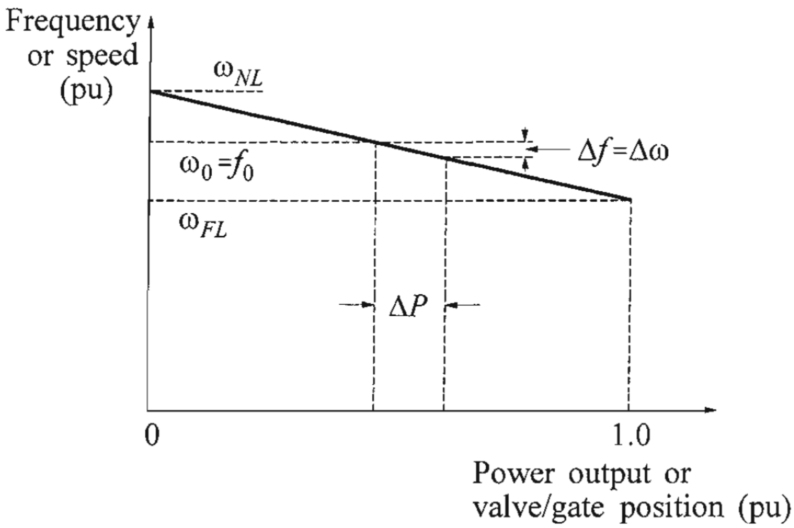

Figure 2.3: Governor droop control characteristics [8]

In this Figure 2.3, it can be seen that as the frequency falls due to increase in load or generation loss, the governor droop control get activated suddenly by increasing the output power, where the full power output occurs at ω_{FL} indicating the steady-state speed at full load. Moreover, ω_o indicates the rated speed, while ω_{NL} is the steady-state speed at no load. The droop can be defined as the ratio of frequency deviation (Δf) to change in power output (ΔP) as shown in Equation (2.1).

$$R = \frac{\Delta f}{\Delta P} \tag{2.1}$$

- **Secondary control reserve**: This control is automatically activated after the primary control fails to return the frequency back to the nominal magnitude. In this control method, the frequency deviation is normalized using a PI type-controller, and is expected to operate within 30 [s]-15 [min] after disturbance occurrence.

- **Tertiary control reserve**: This is manually activated to support the secondary control during a large disturbance in the system. The tertiary reserve occurs by using economic dispatch of generation, and is expected to operate within 15-60 [min]. The activation time interval for each described control methods is presented in Figure 2.4.

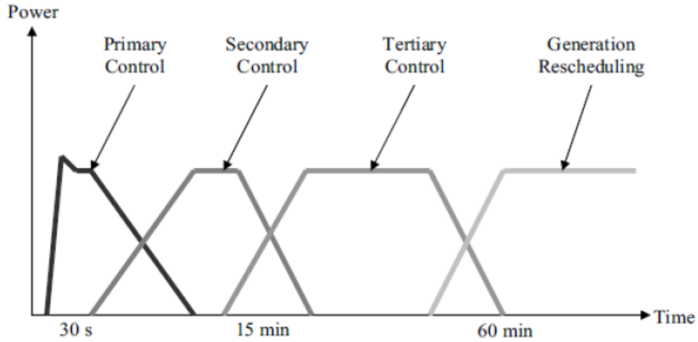

Figure 2.4: Frequency control reserves with their activation time [9]

The control methods described above are commonly applicable in the traditional power system dominated by large-scale of synchronous generators. However, in the modern power system, where the synchronous generation units are increasingly replaced by the converter based generation sources such as WTs and PVs, the system inertia becomes inefficient, which therefore the system frequency becomes more sensitive to the disturbances. Thus, the stability challenges in this situation needs new solutions in order to maintain a sustainable power supply despite the increase of RESs. One of the promising solutions is the BESS and is becoming more attractive and integrated in the power grid due to its various advantages, especially with regards to system frequency stability.
Some type of battery energy storage technologies and their comparisons are provided below.

2.4 Battery energy storage technologies

Battery energy storage technology in power grid is used to store the excess electric power in form of chemical energy during overproduction, and this is later released to grid during peak load. This occurs through chemical reaction process, namely the reduction and oxidation reactions in battery cell. As illustrated in Figure 2.5, a battery cell consists of two electrode, one is a negative also known as anode (Y_O) and another is a positive known as cathode (X_O). Both electrodes are immersed in electrolytic solution called electrolyte (Z), where the anode (Y_O) is coupled with another component of Y_1 while the cathode (X_O) is coupled with X_1 to form two pairs of electrochemically active substances (Y_O-Y_1 and X_O-X_1). The energy difference between those pairs is an indication of the voltage difference between anode and cathode, and when an external load is connected, the battery will start to discharge and therefore the electrons flow from the negative electrode with the maximum energy (anode) to the positive electrode with the minimum energy state (cathode) through oxidation and reduction reactions. The moving electrons and positive ions Y^{2+} are the product of the the oxidation reaction between Y_O and Y_1, while X^{2-} resulted from reduction reaction between X_O and X_1.

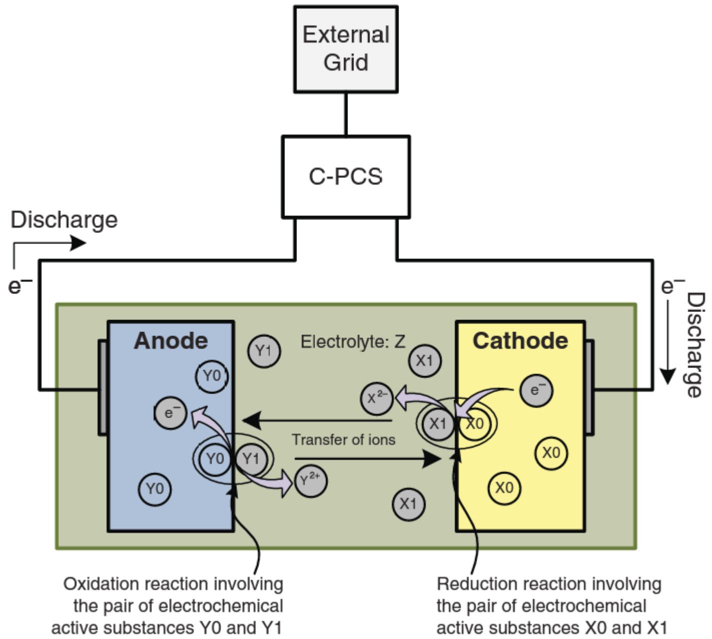

Figure 2.5: Overview of working principle of a battery [10]

The most popular battery technologies such as lead-acid batteries, lithium-ion batteries, Vanadium redox battery and sodium-sulfur batteries are to be described.

2.4.1 Lead-Acid Batteries

The lead-acid batteries have been used for over 100 years, and are still widely used in various applications. They provide a number of advantages like low cost and high efficiency. The working principle of lead-acid battery is mainly based on a positive electrode that is lead dioxide anode (PbO_2), a negative electrode that is sponge lead cathode (Pb) and used electrolyte that is sulfuric acid solution (H_2SO_4). During discharging process of a lead-acid cell, both the oxidation reaction given in Equation (2.2) and the reduction reaction given in Equation (2.3) occurs at the anode and cathode respectively, and the overall reaction can be seen in Equation (2.4). These chemical reactions occur in the reverse direction when the lead-acid cell is recharging [10].

$$Pb + {SO_4}^{2-} \Leftrightarrow PbSO_4 + 2e^- \tag{2.2}$$

$$PbO_2 + 4H^+ + SO_4^{2-} + 2e^- \Leftrightarrow PbSO_4 + 2H_2O \tag{2.3}$$

$$Pb + PbO_2 + 2H_2SO_4 \Leftrightarrow 2PbSO_4 + 2H_2O \tag{2.4}$$

2.4.2 Lithium-Ion batteries

Lithium-ion (Li-Ion) batteries are among the most used battery technologies in various applications and are becoming more attractive in the field of renewable generation since they provide various benefits like higher energy density, quick response and light weight. A Li-Ion cell consists of a positive electrode that is usually lithium metal oxide ($LiCoO_2$), a negative electrode that is carbone (C) and lithium-based dissolved salts that is used as electrolyte. Both electrodes are separated by an insulator made of polyethylene. The reversible chemical reactions that occurs during discharging/charging of a Li-Ion cell at anode and cathode can be seen in Equation (2.5) and (2.6) respectively and the overall reaction is given in Equation (2.7) [10].

$$Li(C) \Leftrightarrow Li^{+} + e^{-} \tag{2.5}$$

$$Li^{+} + e^{-} + CoO_2 \Leftrightarrow LiCoO_2 \tag{2.6}$$

$$Li(C) + CoO_2 \Leftrightarrow LiCoO_2 \tag{2.7}$$

2.4.3 Vanadium Redox Flow Battery (VRFB)

The vanadium redox battery is a type of flow battery technologies, and this differs from the conventional batteries by the fact that the electrolyte is stored in two aqueous electrolytic solutions rather than cells. The VRFB possesses various benefits like very fast response, long lifetime and storage time. VRFB's active elements comprise two electrodes made of catalyzed graphite, and the used electrolytes of sulfuric acid (H_2SO_4). The chemical reactions that occurs during charging/discharging of VRFB cell at anode, cathode are given in Equations (2.8) and (2.9), while the total reaction is given in Equation (2.10) respectively [10].

$$V^{2+} \Leftrightarrow V^{3+} + e^{-} \tag{2.8}$$

$$VO_2^{+} + 2H^{+} \Leftrightarrow VO^{2+} + H_2O \tag{2.9}$$

$$V^{2+} + VO_2^{+} + 2H^{+} \Leftrightarrow V^{3+} + VO^{2+} + H_2O \tag{2.10}$$

2.4.4 Sodium-Sulfur Batteries

These type of sodium-sulfur batteries are more attractive to stationary high-power applications. They provide some benefits like high power density, long lifetime and high efficiency, however one of their drawbacks is their operating conditions at higher temperature to dissolve the sodium. The working principle of sodium is based on a negative electrode that is liquid sodium immersed in electrolyte that is ceramic beta-alumina and the positive electrode of liquid sulfur. These electrodes are then melted with an imposed NaS temperature within $300-400$°C. The operation process of the NaS battery occurs through the chemical reactions at anode given in Equation (2.11) and cathode in Equation (2.12), and the complete reaction can be seen in Equation (2.13) [10].

$$2Na \Leftrightarrow 2Na^{+} + 2e^{-} \tag{2.11}$$

$$xS + 2e^{-} \Leftrightarrow S_x^{2-} \tag{2.12}$$

$$2Na + xS \Leftrightarrow Na_2S_x \tag{2.13}$$

The characteristics of battery energy storage technologies previously described in this section and other storage technologies are presented in Figure 2.6, where they are compared based on their discharging time, MW power scale and efficiency.

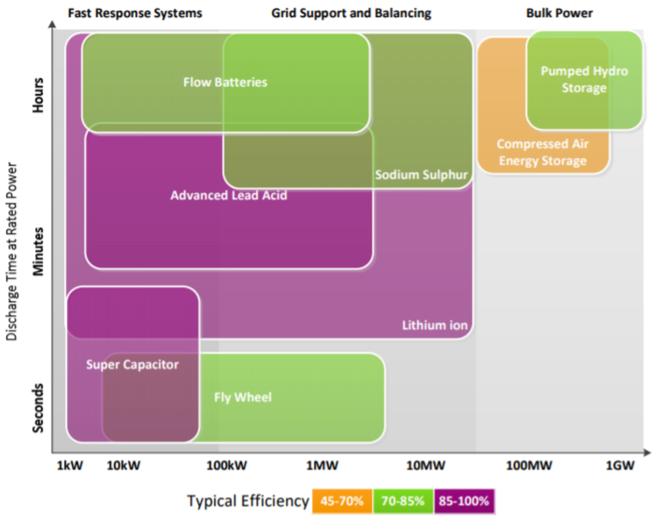

Figure 2.6: Characteristics of various storage technologies [11]

The x-axis in Figure 2.6 represents the discharging time at rated power while the y-axis represents the power scale and the colors shows the efficiency range of the given type of storage. Based on the given characteristics of batteries in Figure 2.6, it can be observed that the Li-Ion and flow batteries have larger power scale with higher discharging time when compared to lead acid and sodium sulphur (NaS) battery. Based on this information, it is obvious that both Li-Ion battery and flow batteries can be good choices and can be applied to support the stability in the system. However, the installed battery type at Livø is Vanadium Redox Flow Battery (VRFB) with 5 [kW] power rating and 40 [kWh] energy rating, and this is one of flow battery types, thus it is considered as the suitable battery energy storage technologies in this project. The basic understanding about power management in battery and its electronic features are described in next subsection.

2.4.5 The battery and power management

The battery application onto power grid is executed with electronic features, mainly the power conversion system (PCS) and battery management system (BMS). The major role of the PCS is to process and direct the power between the battery and the utility grid. The BESS can only store or supply the power in DC form, while the power in the most utility grid is in AC-form. Hence, the PCS with bidirectional ability is applied between the battery and grid to execute a dual-function, either converting DC power into AC power or vice versa.

The BMS's role is to control the power flow within the BESS during charging or discharge depending on the battery condition. In addition, the BMS is used to exchange the critical information about the battery like temperature, bus voltage to the PCS. To estimate the state of charge (SOC) of battery, the BMS needs the measured data of cell temperature, voltage&current, as well as the information of battery age and the number of charge/discharge cycles [12].

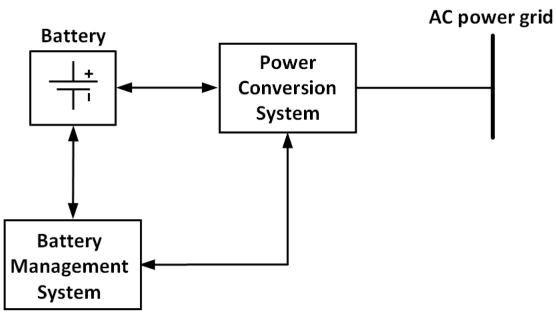

Figure 2.7: Basic structure diagram of BESS

The above Figure 2.7 gives a picture of the interconnection between the battery and power electronic systems, namely the PCS and BMS.

In order to effectively apply the BESS technology onto grid, it is important to be aware of the grid code requirements, thus this is provided in the following section.

2.5 The grid code requirements

Any power grid is designed with a range of technical specifications by which any equipment must comply with before being connected to that grid in order to ensure the stability into power system. The considered requirements in this project are based on the Danish DSOs as provided by Energinet [13]. This dictates the operating frequency to remain stabilized at nominal value of 50 [Hz], and the considered operating limits of range $47.5 \leq f \leq 51.5$ [Hz] as stated in Table A.3. When stabilizing the system frequency using the BESS control, the active power is absorbed or delivered to the grid following the droop control characteristics within the frequency range of $[49.8 - 50.2]$ [Hz] as illustrated in Figure 2.8.

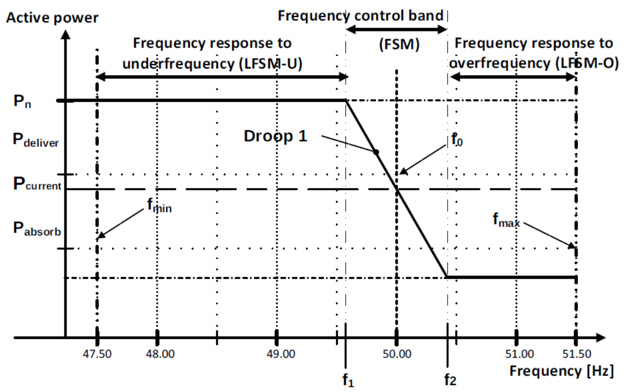

Figure 2.8: Schematic of frequency response by ESS to the system frequency deviation [13]

Table 2.2: Frequency operating limits

-	f_{min}	f_{max}	f_0	f_1	f_2
Frequency Magnitude[Hz]	47.5	51.5	50	49.8	50.2

The frequency values of f_0, f_1, f_2, f_{min} and f_{max} are given in Table 2.2.

Where:

f_0 is ideal base frequency

f_1 denotes Lower frequency threshold which delimits the frequency sensitive mode (FSM) band and is where the autonomous frequency response LFSM-U is initiated

f_2 denotes upper frequency threshold which delimits the FSM band and is where the autonomous frequency response LFSM-O is initiated

f_{min} and f_{max} denote the minimum and maximum frequency within the frequency band respectively.

In this chapter, it is given the overview of microgrid and the power management in the Livø energy system. Moreover, various battery energy storage technologies are investigated, where the Li-Ion and flow batteries are found to have higher potential compared to other type of battery. Furthermore, a basic description on the battery power management is provided, as well as the grid requirements with regards to system frequency limits for BESS connection to the grid.

The model of the power system components and the system simulations are to be examined in the next chapter.

3 | Modelling of the components in Microgrid

In order to develop an appropriate BESS control strategy for system frequency in microgrid, it is important to first examine the used components into microgrid. This chapter will cover the model of the DERs such as DG, WT, PV and BESS. Furthermore, the system network is simulated to examine the frequency behavior before and after connecting the WT and PV into the system.

3.1 Diesel Generator (DG)

DG plays an important role due to the islanded nature of the Livø grid that also contains wind and solar installations. This is due to its major role in ensuring the frequency stability through its inherent control reserve especially inertia reserve. In Figure 3.1, it is shown the block diagram of diesel generator characterised by four main components such as synchronous generator (SG), a diesel engine, a governor and excitation system. Each of these components in diesel generator set is used to provide the required power and also to maintain the system stable and reliable. This is only achieved by ensuring the system frequency and voltage to operate within the allowed limits in the grid. Thus, the governor is used to provide the speed control for diesel engine and thereby the system frequency in grid. In addition, the voltage in grid needs to operate in certain range, and this is ensured by the excitation system through the automatic voltage regulator (AVR).

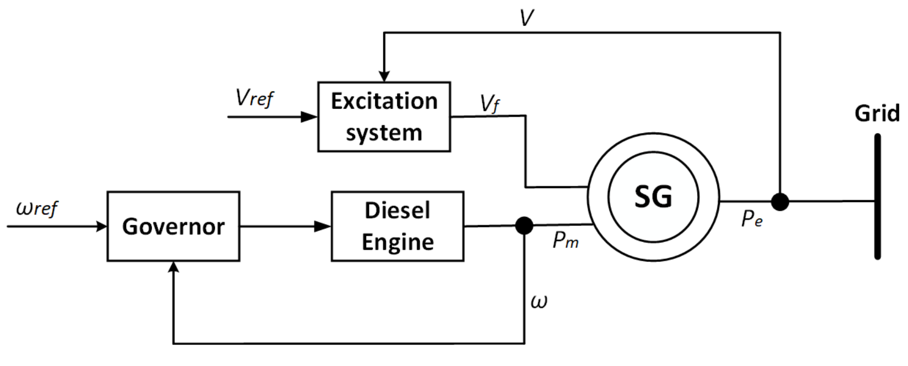

Figure 3.1: Configuration diagram of a diesel generator set

The DG set component models are described in the following subsections.

3.1.1 Governor

In order to execute the task of speed control for engine, the governor control needs to be provided with the suitable parameters. It can be noted that the used governor for the DG set is a standard control model existing in DIgSILENT PowerFactory called degov1. This consists of an electric speed sensor, a hydro-mechanical actuator and the diesel engine as it is shown in Figure 3.2. In addition, the settings for degov1 are provided in Table 3.1.

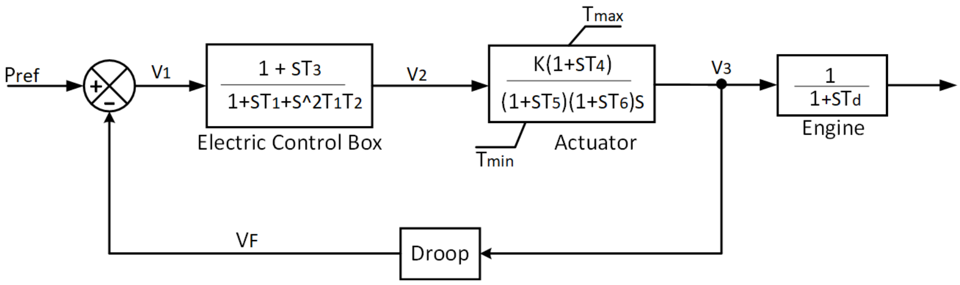

Figure 3.2: Block diagram of governor, DEGOV1

Name	Value
K Actuator gain[pu]	18
T_1 Electric control box first time constant[s]	0.01
T_2 Electric control box second time constant[s]	0.01
T_3 Electric control box derivative time constant[s]	1
T_4 Actuator derivative time constant[s]	0.02
T_5 Actuator first time constant[s]	0.01
T_6 Actuator second time constant[s]	0.01
T_D Combustion Delay[s]	0.02
Droop [pu]	0.008
T_{min} [pu]	0
T_{max} [pu]	1.1

Table 3.1: The used governor specifications.

Where v_1, v_2, v_3 and v_F indicates the input/output signals.

The impact of the electric control box in the system can be examined by analysing the frequency responses of the system. With the settings defined in Table 3.1, the open loop and closed loop transfer function can be obtained as given in Equation (3.1) and (3.2) respectively.

$$G_{ol}(s) = \frac{0.00288 \cdot s^2 + 0.1469 \cdot s + 0.144}{1 \cdot 10^{-8} s^5 + 3 \cdot 10^{-6} \cdot s^4 + 0.0004 \cdot s^3 + 0.03 \cdot s^2 + s} \tag{3.1}$$

$$G_{cl}(s) = \frac{0.36 \cdot s^2 + 18.36 \cdot s + 18}{1 \cdot 10^{-8} s^5 + 3 \cdot 10^{-6} \cdot s^4 + 0.0004 \cdot s^3 + 0.03288 \cdot s^2 + 1.147 \cdot s + 0.144} \tag{3.2}$$

The bode plot for G_{ol}(s), G_{cl}(s) and G_c(s) of electric control box are presented in Figure 3.3. With the open loop bode diagram, the gain margin with −180 [deg] crossover is obtained as 24.8 [dB], while the corresponding phase margin at 0 [dB] is obtained as 98.2 [deg] indicating a stable system, therefore the used parameters are suitable for the governor control, degov1.

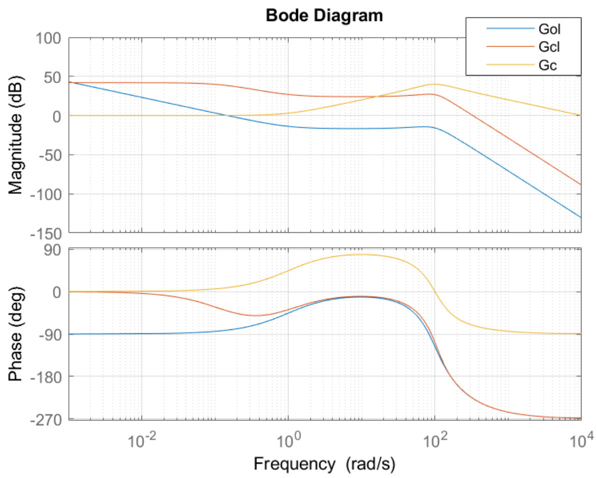

Figure 3.3: Bode plot of open loop($G_{ol}(s)$), closed loop($G_{cl}(s)$) and controller($G_c(s)$)

3.1.2 AVR

As previously mentioned, the AVR provides control to the generated voltage by synchronous generator. The used AVR model in this project is a standard model called IEEET1 in DIgSILENT PowerFactory. The voltage stability is vital in power grid especially an islanded microgrid, and thus the suitable parameters are needed for a better AVR operation. The considered AVR model for DG set can be seen in Figure 3.4. In addition, the used AVR specifications are presented in Table 3.2.

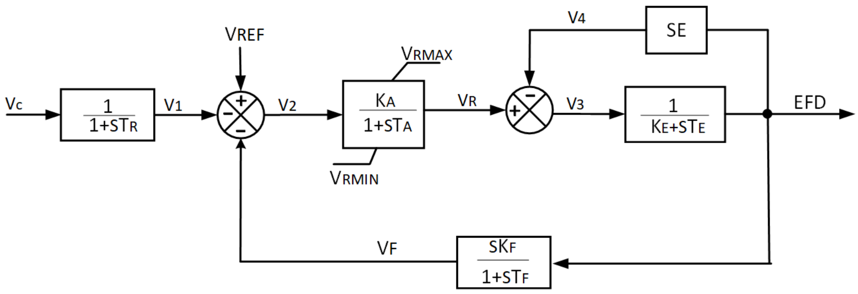

Figure 3.4: Schematic of AVR model

Name	Value
K_A Controller gain[pu]	175
T_R Measurement Delay[s]	0.028
T_a Controller time constant[s]	0.02
K_E Exciter constant[pu]	1
T_E Exciter time constant[s]	1.2
K_F Stabilization path gain[pu]	0.05
T_F Stabilization path time constant[s]	1.5
E_1 Saturation factor1 [pu]	6.5
SE1 Saturation factor2 [pu]	1.5
E_2 Saturation factor3 [pu]	6
SE2 Saturation factor4 [pu]	2.46
V_{min} Controller output minimum[pu]	-12
V_{max} Controller output maximum[pu]	12

Table 3.2: The used AVR specifications.

3.2 Wind turbine

The power generated by the WT depends on different factors, but mainly the wind speed and the swept area of the turbine. In this project, the modelled WT has 25 [kW] of power rating, and the active power is calculated using the equation 3.3 [14].

$$P_{WT} = \frac{1}{2}\rho A V^3 C_p \tag{3.3}$$

Where ρ is air density, A area swept by blades, V is wind speed, C_p is rotor power coefficient. The WT type applied in the system is SWP-25 [KW] produced by Solid Wind Power A/S [15], and this is characterised by its high efficiency, long lifetime and low level of noises. The power flow for this type of WT at different wind speeds can be seen in Figure 3.5.

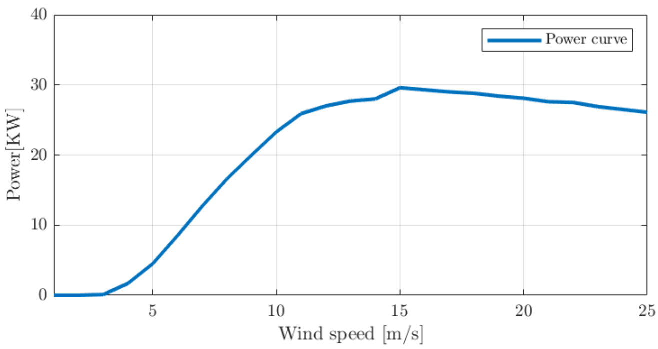

Figure 3.5: The WT's active power at different wind speed.

As indicated by the power curve in Figure 3.5, it can be seen that the considered WT model starts generating the active power when the wind speed reaches 3 [m/s] and there is no power generation when the wind speed is higher than 25 [m/s]. The WT model in this project is based on the calculation executed using the equation 3.3, and the used wind speed data are extracted from the DTU climate station data [16]. In addition, the WT specifications used in the WT power calculation are given in Table 3.3.

Name	Value
Wind speed range(V)	[3-25] [m/s]
Swept Area(A)	154 [m^2]
Wing radius(r)	7 [m]
Power Coefficient (C_p)	0.26
Air density(ρ)	1.23 [kg/m^3]

Table 3.3: WT specifications [15].

3.3 PV

The used PV system model in this project is a standard model in DIgSILENT PowerFactory. The generated power is mainly based on the provided irradiance data and time. This is calculated using the equations 3.4 and 3.5 [17].

$$P_{panel} = \frac{E_{g,pv} P_{pk,panel} \eta_{rel} \eta_{inv}}{E_{STD}} \tag{3.4}$$

$$P_{system} = P_{panel} num_{panels} \tag{3.5}$$

Where:

- P_{panel}: Active power output of the panel in [kW]
- P_{system}: Single system active power output in [kW]
- num_{panels}: Number of panels per inverter
- $E_{g,pv}$: Global irradiance on the plane of the array in W/m^2
- E_{STD}: Standard irradiance value of $1000 W/m^2$
- $P_{pk,panel}$: Total rated peak power of the solar panel in [kW]
- η_{rel}: Relative efficiency of the panel
- η_{inv}: Efficiency factor of the inverter

The used irradiance data in the model are provided by PV outdoor test and monitoring platform, AAU energi, Aalborg University. The selected irradance profile in the model are chosen according to the consumption level at Livø. The chosen day with low consumption is the 02.May.2012, where during high consumption is the 30.October.2012. The irradiance profile for both cases are presented in Figure 3.6 and 3.7 respectively. The further description of the PV model can be seen in Appendix A.2.

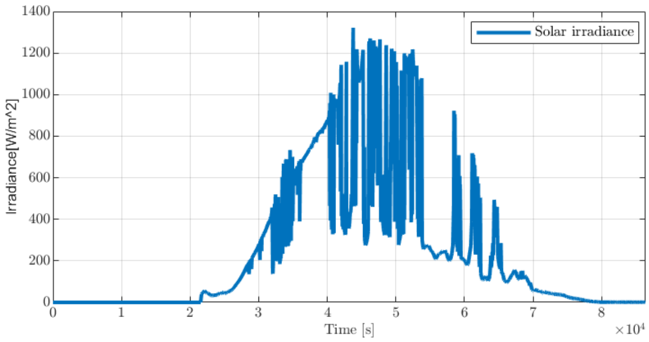

Figure 3.6: The solar irradiance profile on 02-May-2012

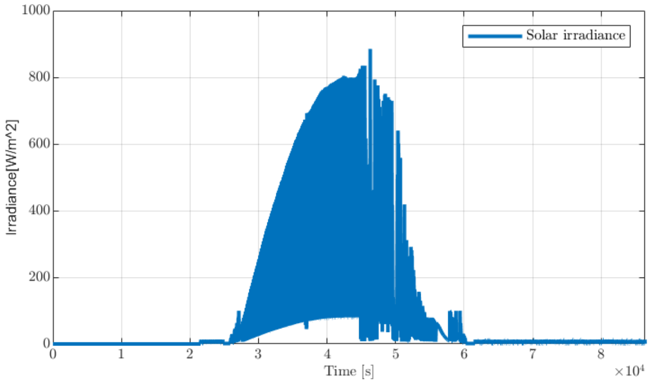

Figure 3.7: The solar irradiance profile on 30-October-2012

From Figure 3.6 and 3.7, it is observed that between $(0-2.15)\cdot10^4$ [s] or [00 : 00 − 06 : 00] the irradiation is around 0 $[\frac{W}{m^2}]$ since there is no sunlight during night, which means that no PV power generation occurs during this time, and thus the BESS is expected to discharge the power to grid. However, between $(2.15-7.6)\cdot10^4$ [s] or [06 : 00 − 21 : 00], the irradiation is observed to increase as there is sunlight, which means the increase of PV power generation, therefore the BESS is expected to charge the surplus power in this time.

3.4 Hot water storage tank

The Livø grid contains el-boiler associated with a large hot water storage tank (HWST). The DG is a CHP plant, where the heat is stored in this HWST and also the excess electricity from renewable resources is to be stored in the form of heat in HWST. The heating system is not investigated in this project, however it is important to determine the storage time and the rated energy capacity of the storage tank based on its specifications and the used el-boiler capacity. The utilized storage tank has a volume of 32000 liters, where this is equivalent to 32000 [kg]. In addition, the specific heat of water or C_P is 4180 $[\frac{kj}{kg°C}]$, hot water temperature or T_{water} is 85 [°C] and the surrounding temperature or T_{srnd} is 30 [°C]. From these given data, the energy rating of storage tank can be determined by using the Equation (3.6).

$$E_{rate} = m \cdot C_P \cdot (T_{water} - T_{srnd}) \cdot \frac{1}{3600} \tag{3.6}$$

Thus, the energy rating of storage tank in Equation (3.6) is obtained as 2043.6 [kWh]. Moreover, by using the Equation (3.7), it is found that with the el-boiler of 67.5 [kW] power rating, the storage time is determined to be around 30 hours.

$$t = \frac{E_{rate}}{P_{elboiler}} \tag{3.7}$$

3.5 BESS model

The BESS model in this project is expected to replace the primary control reserve of the DG with the purpose of reducing the usage of the DG and the consumption of fossil fuels in the system.
The BESS system consists of 3 main components:

- Battery
- Converter
- BESS controller

3.5.1 Battery

The battery is a storing device of the BESS, where the charged power is stored in form of chemical energy, and this energy is then released in form of electric power when it is needed. The developed battery model has 40 [kWh] energy rating and 5 [kW] power rating. It can be emphasized that the battery in this project is modelled as the voltage source, because the Vanadium Redox Flow battery model is not available in PowerFactory at the moment. The battery is dimensioned using the Equation (3.8), (3.9) and (3.10), and the used specifications can be found in Table 3.4.

$$V_{cell} = V_{max} \cdot SOC_O + V_{min} \cdot (1 - SOC_O) \tag{3.8}$$

$$V_{term} = \frac{V_{cell} \cdot n_{row}}{1000} \tag{3.9}$$

$$E_{batt,rate} = C_{Cell} \cdot n_{parallel} \cdot V_{term} \tag{3.10}$$

Table 3.4: Battery settings

Name	Value
SOC_O	0.5
V_{min}	12 [V]
V_{max}	13.85 [V]
$n_{parallel}$ (Cells in parallel)	12
n_{row} (Cells in row)	65
V_{nom}	0.9 [kV]
$R_{i,cell}$	0.001 [Ω]
$I_{inputSignal}$	1 [kA]
C_{Cell}, Capacity per cell	4 [Ah]

3.5.2 Converter

The converter component is used to facilitate the power exchange between the BESS and grid, where it converts the DC-power on battery side to AC-power on grid side and vice versa. The used converter model is standard model of an IGBT-based voltage source converter (VSC) with PWM in PowerFactory.

3.5.3 BESS controller

The BESS model comprises of controllers that ensure the reliable operation of battery and PWM converter in accordance with the condition of grid. The used controllers are PQ controller, charge controller and frequency controller.

- *Frequency controller:* This controller receives the measured frequency signal from grid through the PLL. Within the frequency controller, the droop is set as 0.004 [pu] and the deadband is set to be 0.0004 [pu]. In this case, the deadband indicates that there will be no control activation for the frequency magnitude within range of [49.98 – 50.02] [Hz], whereas the given droop indicates that the full active power will be activated when the frequency deviation is greater or equal to 0.2 [Hz].
- *PQ controller:* This controller aims to adjust the active power as well as the reactive power in BESS based on the signal generated from the frequency controller and the measured power and voltage in grid.
- *Charge controller:* This controller determines the charging and discharging condition of BESS based on the information received from PQ controller as well as the SOC level available in battery.

In Figure 3.8, the configuration of the BESS model and the input&output signals for each component are shown. The PLL block is used to detect the frequency magnitude using the voltage in grid, the output signal leads to frequency controller block. This controller converts the input signal to the power reference that is then used as the input to the PQ controller. In this PQ controller, the power references together with voltage reference are compared to the input signals measured from grid, and the differences are processed to generate the actual i_{dref} and i_{qref} signals which stands for the active and reactive power respectively. These output signals leads to charge controller that ensures the charging conditions of the battery based on the predefined boundary conditions as wells as the input signals from PQ controller. The further descriptions and specifications of BESS controllers are provided in Appendix A.1.

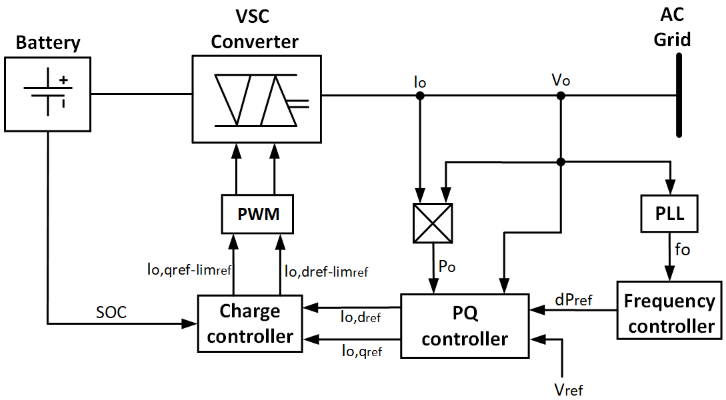

Figure 3.8: Schematic diagram of BESS model

3.6 BESS control strategy

To maintain the grid frequency within the defined limits using BESS, it is needed to develop and implement a suitable control strategy for the BESS. This BESS control strategy is expected to ensure the fast response to any frequency deviation that may occur due to either overproduction or peak-load. The BESS in this project is expected to replace the primary frequency control of the DG. Therefore, as shown in Figure 2.8, the BESS control is expected to activate the full active power when the frequency deviation is greater or equal to 0.2 [Hz]. In addition, the dead-band is set to be 0.0004 [pu] which means that the BESS control is first activated if the frequency deviates from the interval of 49.98 – 50.02 [Hz]. These characteristics of the BESS control operation are gathered in Figure 3.9.

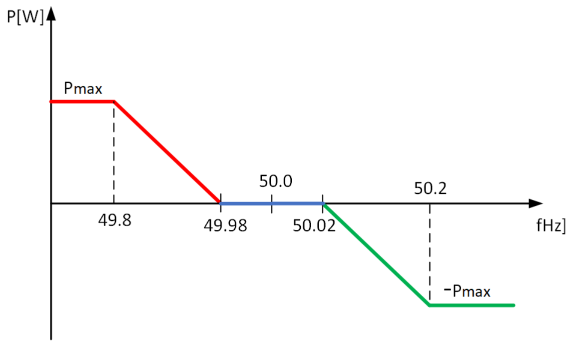

Figure 3.9: Frequency response by BESS control

The Figure of 3.9 indicates the deadband range of 49.98 – 50.02 [Hz] where there is no reaction of BESS control. However, for the frequency within 49.8 – 49.98 [Hz], the upward-regulation of BESS control is activated, while the downward-regulation is activated for the frequency within 50.02 – 50.2 [Hz] interval. In accordance with those BESS control operating condition lately described as well as the charging boundary condition of the battery, the BESS control strategy is developed as shown in Figure 3.10.

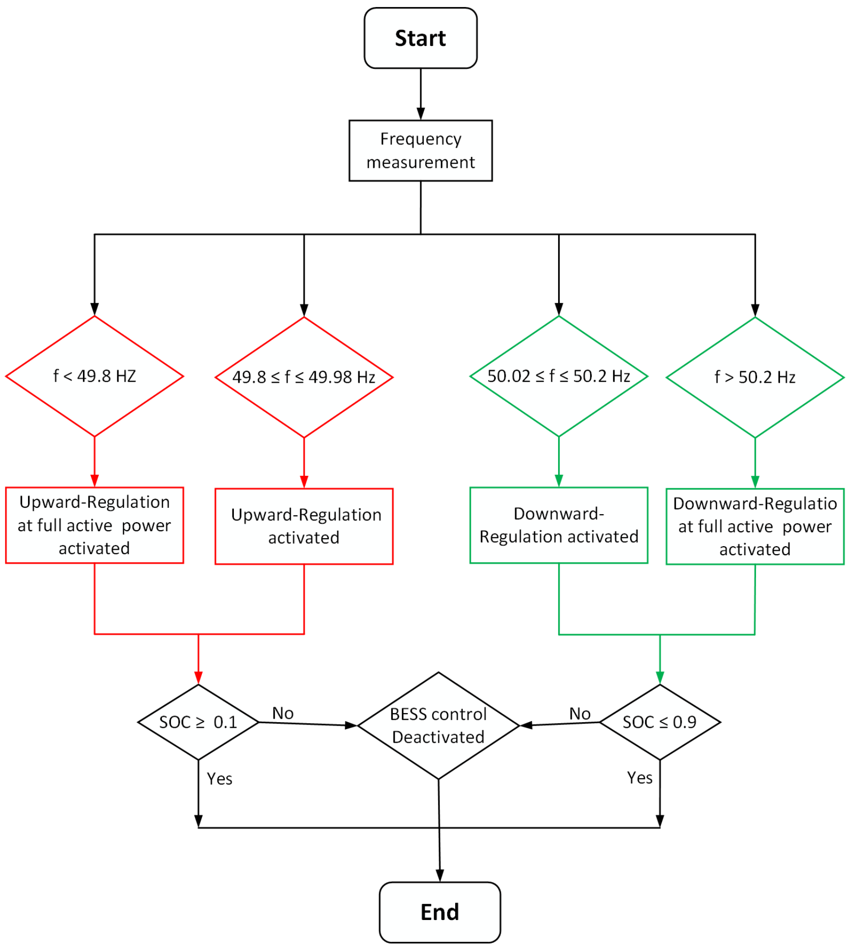

Figure 3.10: The flow chart of BESS control strategy for frequency stability.

The battery SOC normally varies within $0\% \leq SOC \leq 100\%$ or $0 \leq SOC \leq 1$. However, to increase the battery lifetime and efficiency as well, it should not be fully charged/discharged. In this case, the SOC is therefore set to operate within $10\% \leq SOC \leq 90\%$ or $0.1 \leq SOC \leq 0.9$. The flow chart for the developed BESS control strategy is shown 3.10. It can observed that the frequency in grid is first measured, where it leads to one of the 4 possible options of frequency constraints. These constraints can be classified into two group, where the first group consists of two options marked in red and in this particular case, the upward-regulation of BESS control is activated. Afterwards, the SOC level in battery is checked before releasing the power to grid. In case the $SOC \geq 0.1$, the requested power is delivered to grid, otherwise the BESS control is deactivated since there is not enough power in BESS. The second group also consists of two options marked in green, where in this particular case, the down-regulation of BESS control is activated. Afterwards, the SOC level is checked and if this is less than 0.9, the battery will start to absorb the active power from grid, otherwise the BESS control is deactivated since the battery's SOC has reached the allowed maximum value.

3.7 Livø power system network

Before examining the developed BESS control strategy in previous section, it is needed to first investigate the operating condition of the considered power system network of the Livø island. As it can be seen in Figure 3.11, this system consists of the generation sources which are 3 DGs situated at GB1-bus, WT placed at B2-bus, PV placed at B10-bus and the storage device of BESS placed at B9-bus. In addition, the system consists of 18 different actual loads distributed throughout different buses, 2 heat pumps(HP) at B2-bus and 1 el-boiler placed at B3-bus. The DG provides both inertia and primary control reserve needed to maintain the frequency within the admissible limits. However, the BESS control strategy to be implemented in this system is expected to replace the DG primary control reserve with the aim of reducing the usage of DG while prioritizing the RESs. The HP and el-boiler are used to ensure the balance between generation and production by consuming the surplus power resulted from WT and PV. The used specifications for each component are provided in Table 3.5 and the load profile for the actual loads are given in Appendix B.

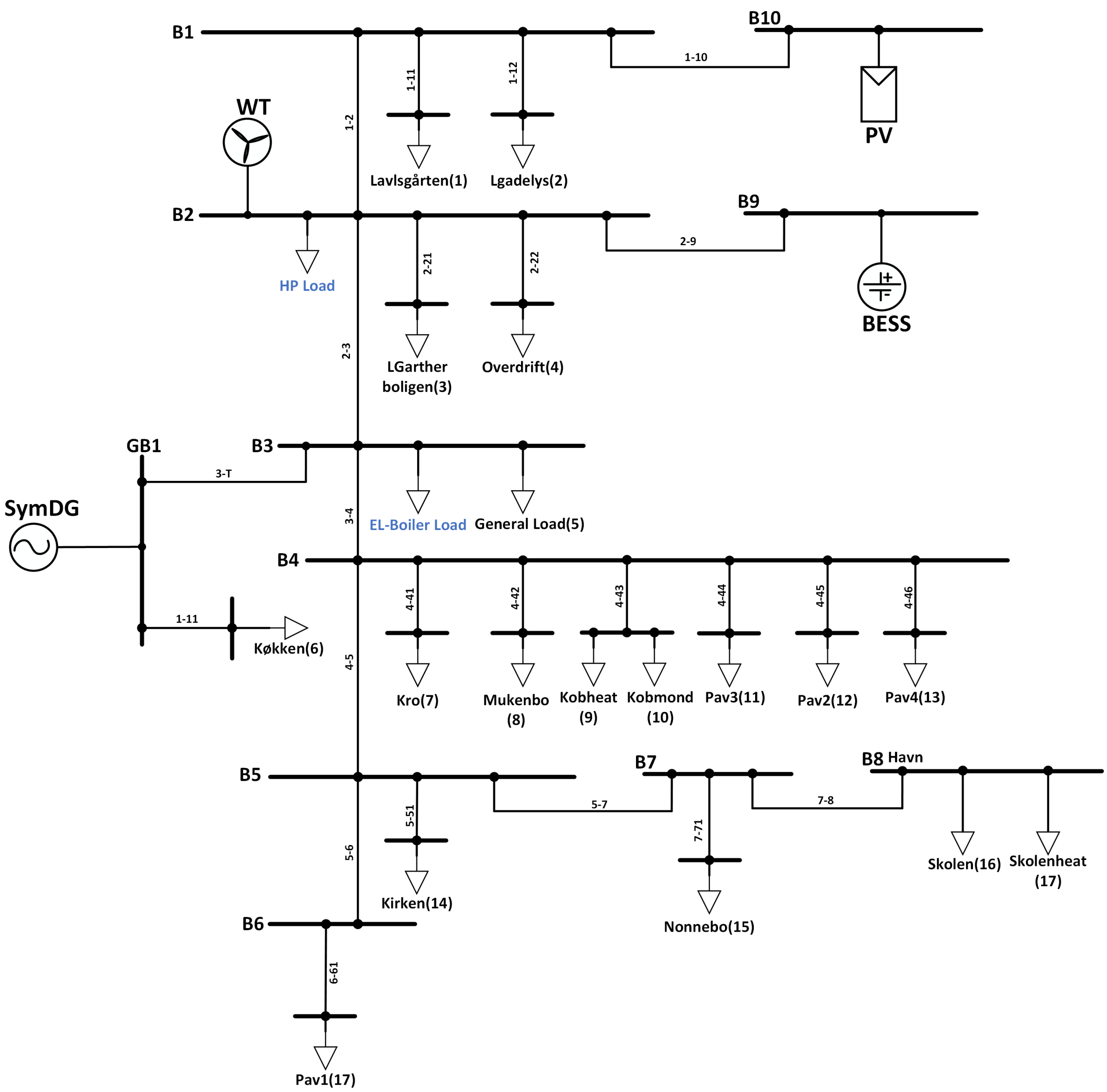

Figure 3.11: The system network model of Livø island

Table 3.5: The system component parameters

Diesel Generator (DG)		
Name	Notation	Value
Rated apparent power	S	0.045 [kVA]
Active power	P	0.036 [MW]
Reactive power	Q	0.027 [MVar]
Rated voltage(rms)	V	0.4 [kV]
Power factor	pf	0.9
Wind Turbine (WT)		
Name	Notation	Value
Rated active power	P	0.025 [MW]
Rated voltage(rms)	V	0.4 [kV]
Power factor	pf	1
Photovoltaic (PV)		
Name	Notation	Value
Rated active power	P	0.033 [MW]
Rated voltage(rms)	V	0.4 [kV]
Power factor	pf	1
Line		
Name	Notation	Value
Res, Cap of Cable(3-T, 1-10)	R, C	0.208 [Ω/km], 0.064 [μF/km
Res, Cap of OHL(1-2, 2-3, 3-4, 4-5, 5-6, 5-7, 7-8)	R, C	0.524 [Ω/km], 0.59 [μF/km]
Res, Cap of Cable(01-011,1-11,1-12,2-21,2-22,4-41, 4-42,4-43,4-44,4-45,4-46,5-51,6-61,7-71)	R, C	1.83 [Ω/km], 0.25 [μF/km
Res, Cap of Cable(2-9)	R, C	1.2 [Ω/km], 0.28 [μF/km]
Load		
Name	Notation	Value
Heat pump	HP	0.0038 [MW]
Electrical boiler	El-boiler	0.0678 [MW]
Battery energy storage	BESS	0.005 [MW], 40 [kWh]

To investigate the working condition of the system model, two study cases both the low and high consumption cases are to be examined. Both cases will be used to assess the frequency behaviour in system under the influence of the RESs. The selected day with low and high consumption are on the 02.May and 30.Oct respectively as shown in the load profile in Appendix B.

The load profile for the whole day during low and high consumption is shown in Figure 3.12.

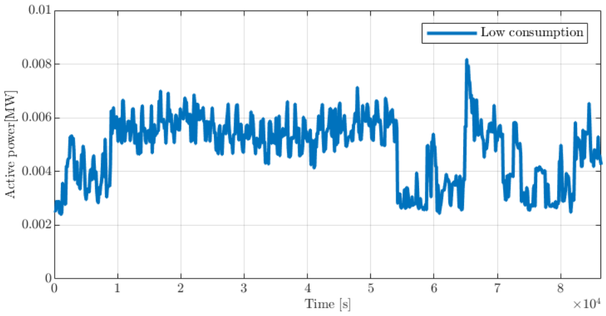

(a) Low consumption

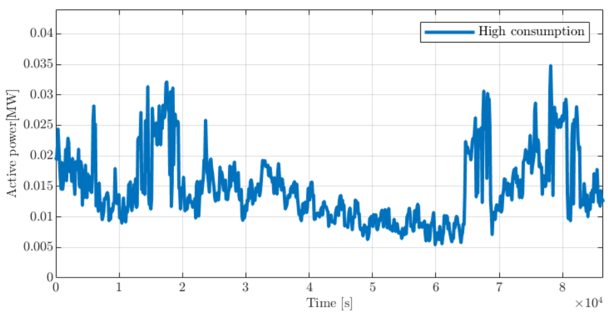

(b) High consumption

Figure 3.12: The load profile during: (a)Low consumption and (b)High consumption

The active power during low consumption in Figure 3.12a varies between 0.0025 to 0.0082 [MW] while the active power during high consumption in Figure 3.12 varies between 0.0055 to 0.035 [MW]. It is evident that the active power during low consumption is observed to be operating under 0.011 [MW] that is the required minimum load for DG operation to stabilize the system network. To increase the load capacity in this case, the HP operating at 0.0076 [MW] is connected to the system and the power extracted from DG is therefore increased and varies between 0.01 to 0.016 [MW] as it can be seen in Figure 3.13. With the DG as the only power source in the system, the simulated frequency during low and high consumption period are presented in Figure 3.14a and 3.14b.

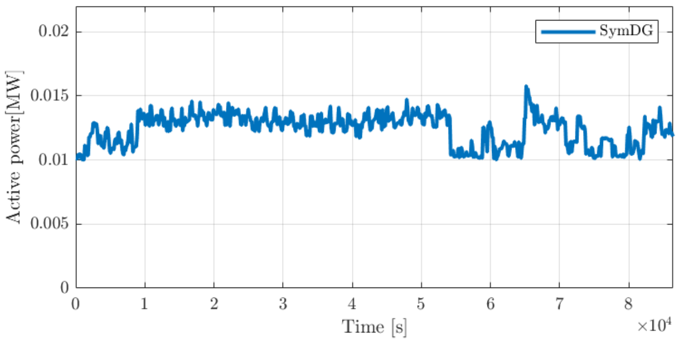

Figure 3.13: Low consumption profile including actual load and HP

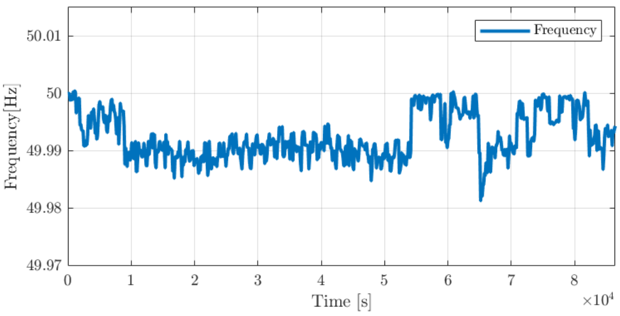

(a) Low consumption

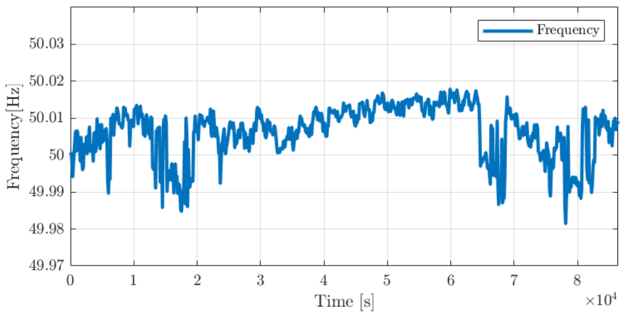

(b) High consumption

Figure 3.14: The system frequency during: (a)Low consumption and (b)High consumption

The frequency behavior shown in Figure 3.14 is the consequence of the load changes in system. By taking a close observation of frequency during low consumption in 3.14a , the frequency is seen to fall in the first 10.000 [s] as the result of the rise in active power of the actual load shown in Figure 3.12a. On the other hand, in case of high consumption, the frequency is seen to rise in the first 10.000 [s] of time as shown in Figure 3.14b due to the increase in actual load demand shown in Figure 3.12b. However, due to the speed governor control and the system inertia of the DG, the frequency is prevented from exceeding the deaband limits in both cases where it is maintained within $49.98 - 50.02$ [Hz] despite the changes in load. From this observation, it can be concluded that the installed DG is able to maintain the system frequency within the defined deadband limits in both low and high consumption cases.
The next step is to integrate the WT and PV in the system aiming to reduce the usage of the DG.
The integration of WT and PV into the system are expected to affect the frequency operation due to various factors like their fluctuating power generation as previously explained. Thus, in order to ensure the system stability with WT and PV integrated, the following two critical scenarios are considered and will be examined in this project.

- *1st scenario*: Low Consumption and High RE
- *2nd scenario*: High Consumption and Low RE

3.7.1 1st scenario: Low consumption and High RE

During this scenario, the system is operating under low consumption while the RE production is high in system. The RE generation causes the reduction of power consumption from DG and the control reserve as well which results into the system instability. To keep the system running, the el-boiler is connected and provided with varying power capacity with respect to the amount of surplus power in system. The consumption profile for actual load, HP and el-boiler are given in Figure 3.15. In addition, the general consumption profile of grid is shown in Figure 3.16, while the generated active power from WT and PV is shown in Figure 3.17.

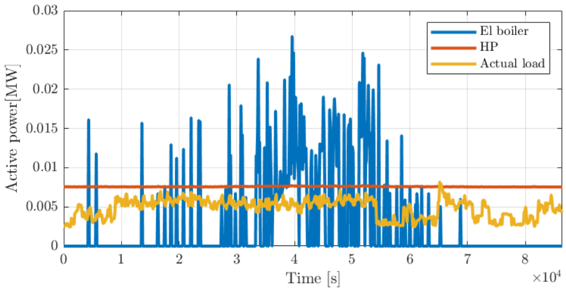

Figure 3.15: Actual load, HP and Elboiler profiles

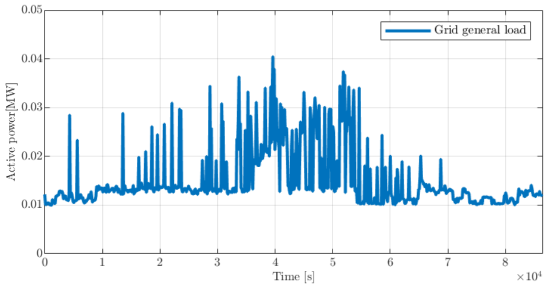

Figure 3.16: Consumption profile in grid that includes Actual load, HP&Elboiler

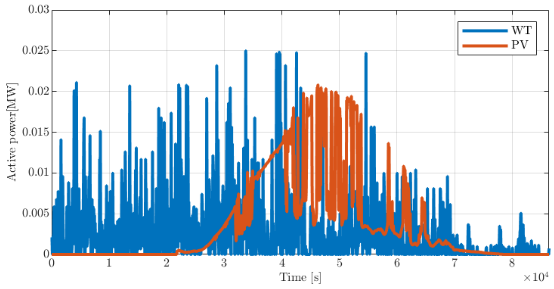

Figure 3.17: The WT&PV during high production

To find out the operating condition of system in this scenario, the system frequency is simulated in Figure 3.18. In this case, it can be observed that the minimum value of frequency is around 49.93 [Hz] while the maximum is measured around 50.16 [Hz]. It is therefore obvious that the used flexible loads that are HP & Elboiler are not able to maintain the frequency withing the deadband limits.

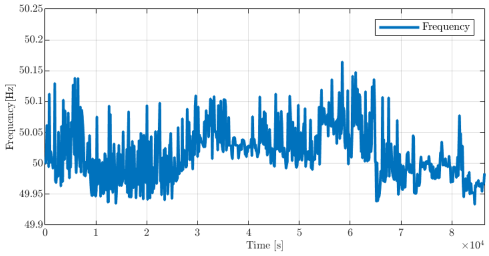

Figure 3.18: The frequency in system with low consumption and high production

3.7.2 2nd scenario: High consumption and Low RE

In this section, it is to examine the operating condition of system when the power demand is high while there is low production from WT & PV. Contrary to the first scenario, the HP and Electric boiler are disconnected since the RE production is low in this case. The simulated grid consumption and WT & PV generation profiles for this scenario are presented in Figures 3.19 and 3.20 respectively.

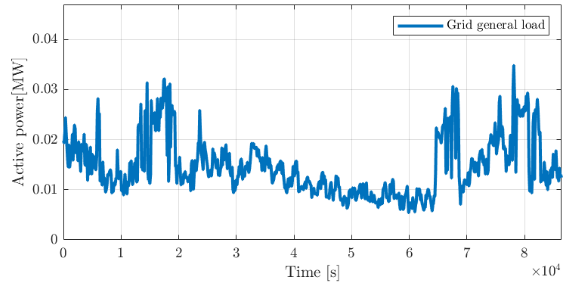

Figure 3.19: High consumption profile in grid

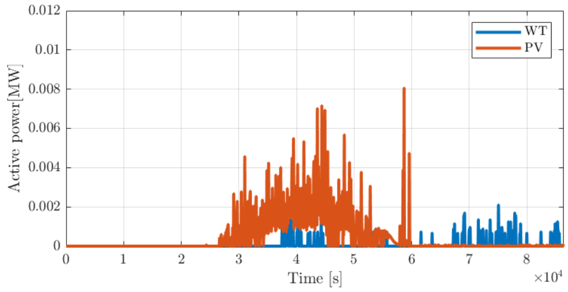

Figure 3.20: The WT & PV during low production

The simulated frequency in this scenario is provided in Figure 3.21. The lowest value of frequency is found to be 49.87[Hz] while the highest value is 50.17 [Hz]. Thus, it is obvious that the frequency has violated the defined deaband interval of [49.98 – 50.02] [Hz].

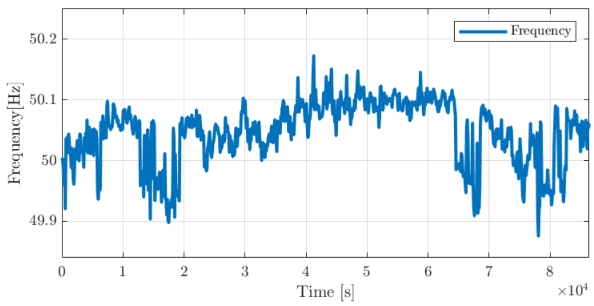

Figure 3.21: The simulated frequency in system
with high consumption and low production

In this chapter, the working models of DG, WT, PV and BESS are provided. Furthermore, the system without RE is examined, where it is found out that the used DG source is able to maintain the frequency within the defined limits. With the aim of reducing the usage of DG, the WT & PV are integrated in the system along with the HP and el-boiler. However, the resulted frequency in the examined scenarios violated the defined limits. To prevent this, the BESS control strategy is to be implemented in the system in Chapter 4, where its main task will be to provide the primary frequency control in the system.

4 | Implementation of the BESS control strategy in the system model

This chapter is aimed to implement the developed BESS control strategy in the system expected to provide the primary frequency control to keep the frequency operating within the allowed limits. This BESS control will be examined in both two scenarios provided in section 3.7.

The developed control strategy is implemented in BESS model placed at Bus B9 in Figure 3.11. This BESS control is intended to play a role of managing the power exchange between the BESS and grid in accordance with the the considered boundary conditions as well as the measured variables into grid. The performance of the BESS control and its impact on the system model is to be evaluated using the two scenarios described in 3.7.1 and3.7.2 through simulations.

4.1 1st scenario: Low consumption and High RE

It is found out in 3.7.1 that the simulated frequency in system operating under low consumption and high RE exceeds the defined dead-band limits of [49.98 – 50.02] [Hz] interval. In this case, before the BESS control is implemented, the maximum frequency is measured to be around 50.16 [Hz] that gives a deviation around 0.14 [Hz], while the minimum frequency is measured to be around 49.93 [Hz] and this gives a deviation around 0.05 [Hz] from the minimal limit of dead-band interval.
With the BESS control strategy implemented in system, the frequency deviation is reduced when compared to the measured frequency without BESS as it can be seen in Figure 4.1. This Figure contains both the simulated frequency without BESS in blue and with BESS in brown. The maximum frequency in system with BESS is measured as 50.11 [Hz], and this corresponds to the deviation of 0.09 [Hz] and the minimum frequency is measured as 49.95 [Hz] and this correspond to the deviation of 0.03 [Hz] from the defined dead-band limit. From this evaluation, it's obvious that the frequency deviation is reduced with BESS control and thus operating as expected. However, the frequency is still violating the allowed limits and this is due to the lower rated capacity of BESS compared to the amount of power needed to be compensated in grid. The active power absorbed from grid to BESS in times of low power demand as well as the delivered power from BESS to grid in times of high demand is presented in Figure 4.2. In addition, the charging and discharging scenarios can be seen in Figure 4.3. In case the measured frequency is lower than 49.98 [Hz], the upward-regulation of BESS control

is activated and this is indicated by the positive active power at BESS ac terminal and a decrease in SOC. On the other hand, when the frequency is greater than 50.02 [Hz], the downward-regulation of BESS control is activated, and therefore the active power at BESS ac terminal becomes negative and the SOC increases. The working condition of the BESS control for this scenario is gathered in Table 4.1. It can be observed that between $(0-0.9)\cdot 10^4$ [s] or $(00:00-02:30)$, the wind speed is high while the consumption is low, thus the downward-regulation dominates which means the battery is charging during this time. Between $(0.9-2.7)\cdot 10^4$ [s] or $(02:30-07:30)$, upward-regulation dominates, i.e. the BESS is discharging, and this is due to consumption rise since it's morning and people turn on light and other domestic devices that consume the electricity. However, the time between $(2.7-7)\cdot 10^4$ [s] or $(07:30-19:30)$ is dominated by downward-regulation, this is caused by higher production from both PV and WT, thus the BESS is absorbing the surplus power during this period. The time between $(7-8.64)\cdot 10^4$ [s] or $(19:30-24:00)$, the upward-regulation dominates, this is due to consumption rise as many people are home in the evening, thus TV, light and other devices are turned on.

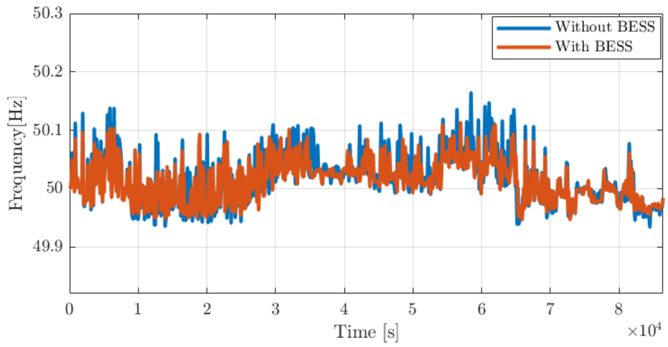

Figure 4.1: The frequency with and without BESS

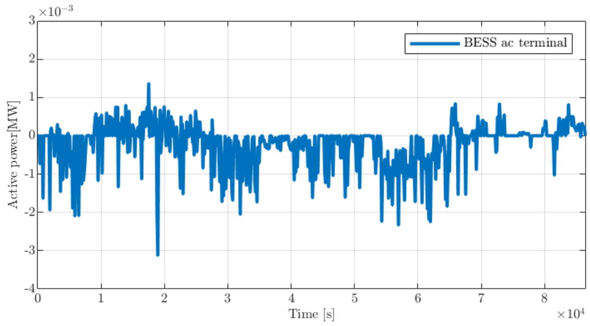

Figure 4.2: The active power at BESS ac terminal

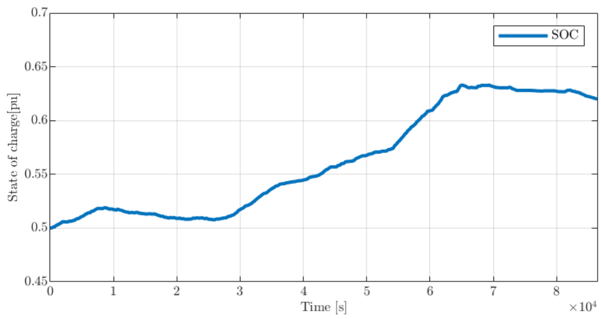

Figure 4.3: The state of charge

Table 4.1: Status of BESS control response to the frequency deviation in the system

Time [s]	BESS Control response	Power at BESS ac terminal	SOC
$(0 - 0.9) \cdot 10^4$	Downward-regulation	Negative	Increasing
$(0.9 - 2.7) \cdot 10^4$	Upward-regulation	Positive	Decreasing
$(2.7 - 3.6) \cdot 10^4$	Downward-regulation	Negative	Increasing
$(3.6 - 4) \cdot 10^4$	Slight downward reaction	Negative	Slight increasing
$(4 - 7) \cdot 10^4$	Downward-regulation	Negative	Increasing
$(7 - 8.64) \cdot 10^4$	Upward-regulation	Positive	Decreasing

4.2 2nd scenario: High consumption and Low RE

The system in this scenario is operating under high consumption during low RE. It is found out in section 3.7.2 that the frequency in system is violating the deadband limits, thus the BESS control in this case is needed to reduce the risks of frequency deviation. The resulted frequency before and after BESS Control is presented in Figure 4.4, where the blue indicate the measured frequency without BESS and the brown indicates the measured frequency with BESS control. In this case, the maximum frequency is reduced from 50.17 [Hz] to 50.14 [Hz] while the minimum frequency is increased from 49.87 [Hz] to 49.91 [Hz] due to BESS control. Therefore, it is obvious that the frequency deviation with BESS Control is less than the frequency deviation without BESS control, however the frequency is still exceeding the dead-band limits. This means that the power that needs to be compensated in grid is higher than the BESS capacity. The active power at BESS ac terminal and the state of charge are shown in Figure 4.5 and 4.6 respectively. The working condition of BESS control is illustrated in Table 4.2. It can be observed the time between $(0 - 1.3) \cdot 10^4$ [s] or $(00:00 - 03:35)$ is dominated by downward-regulation due to low consumption as it is during night. Between $(1.3 - 2) \cdot 10^4$ [s] or $(03:35 - 05:36)$, upward-regulation dominates, thus the BESS is discharging the power to grid. Between $(2 - 6.5) \cdot 10^4$ [s] or $(05:36 - 18:00)$, downward-regulation is activated, and thus the BESS is absorbing the power from grid. Then, the time between $(6.5 - 8.64) \cdot 10^4$ [s] or $(18:00 - 24:00)$, upward and slight downward-regulation are activated.

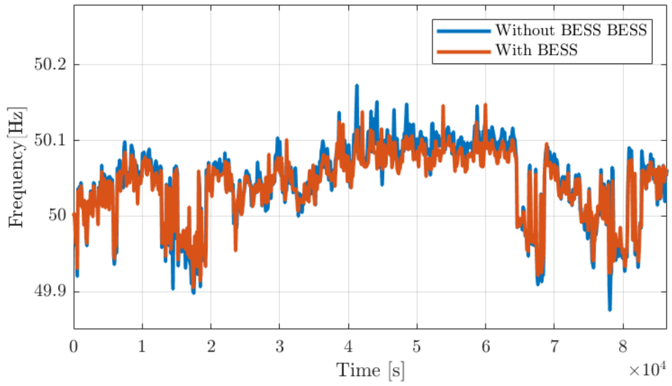

Figure 4.4: The frequency with and without BESS

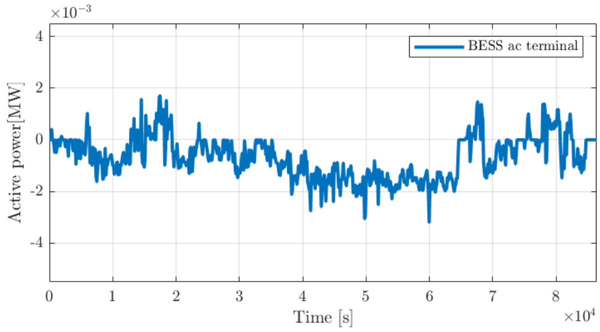

Figure 4.5: The active power at BESS ac terminal

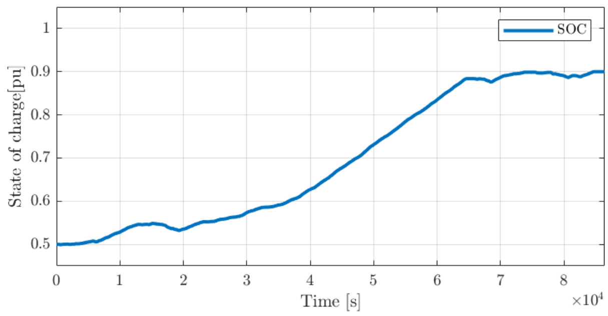

Figure 4.6: The state of charge

Table 4.2: Status of BESS control response to the frequency deviation in the system

Time [s]	BESS control response	Power at BESS ac terminal	SOC
$(0 - 1.3) \cdot 10^4$	Downward-regulation	Negative	Increasing
$(1.3 - 2) \cdot 10^4$	Upward-regulation	Positive	Decreasing
$(2 - 6.5) \cdot 10^4$	Downward-regulation	Negative	Increasing
$(6.5 - 8.64) \cdot 10^4$	Upward&slight downward	Negative&Positive	Increasing&Decreasing

In this chapter, the developed BESS control strategy is implemented and evaluated in both scenarios. It is observed through simulations that the frequency deviation is reduced in system with BESS control. However, it is found out that the BESS is not able to maintain the frequency within deadband limits due to its lower capacity compared to the power needed to be compensated in grid. Therefore, in

Chapter 5, the sensitivity analysis will be carried out in order to find out the suitable size of the BESS.

5 Sizing of BESS for improving the frequency stability

With the considered inverting power rating of 5 *[kW] in Chapter 4, it was evident that the proposed BESS control strategy is unable to maintain frequency within dead-band limits. In this chapter, the suitable size of BESS capacity is determined through sensitivity analysis.*

To maintain the system frequency within allowable limits, it is needed to increase the BESS size to a higher capacity than 5 [kW], so that it may consume extra active power from the system. This is achieved by doing sensitivity analysis for rate of change of frequency with respect to BESS output power. The BESS rated capacity levels to be explored is from 5 [kW] to 35 [kW] with a step-size of 5 [kW], and this is to be performed for two critical scenarios previously described in Chapter 4.

5.1 1st Scenario: Low consumption and high RE

To reduce the frequency deviation in this case, the proper size of BESS is to be determined through sensitivity analysis. The BESS with power rating of 10, 15, 20, 25, 30 and 35 [kW] are applied in the system, and their impacts on the system frequency and state of charge are investigated through simulation.

The simulated frequency for different power rating of BESS on the 02.May is shown in Figure 5.1, where it can be observed that the frequency deviation decreases with increasing power rating.

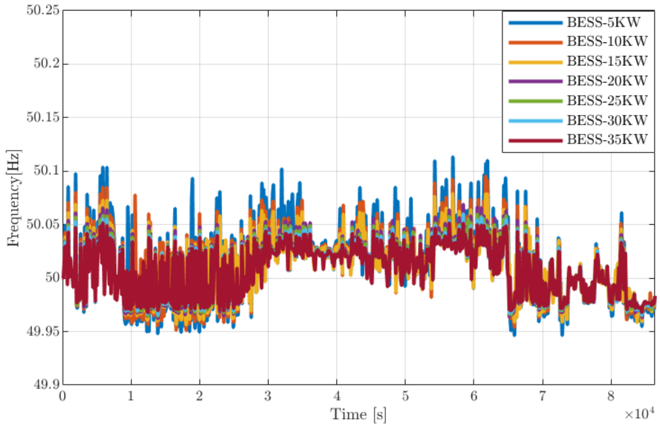

Figure 5.1: Frequency for different BESS power rating

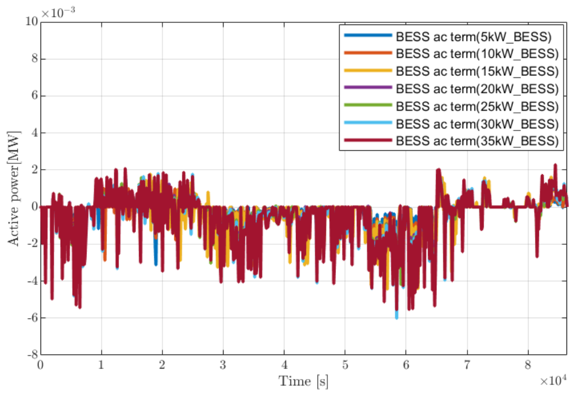

Figure 5.2: Active power at BESS ac terminal

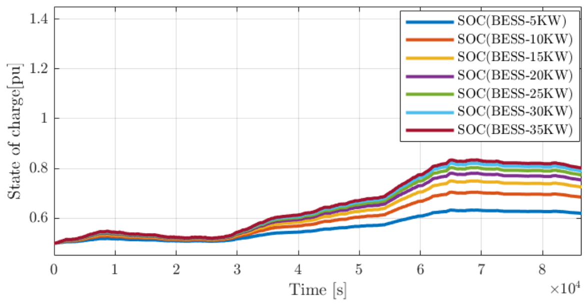

Figure 5.3: State of charge

The impact of power rating on frequency is evaluated by calculating the rate of change using the measured data in Table 5.1. Based on the calculated average rate of change of frequency with respect to the power rating given in that table, it can be seen that the BESS-30 [kW] and BESS-35 [kW] are having the smallest rate of change compared to the rest, therefore the BESS-25 [kW] is selected as the suitable BESS size in this case. The rate of change (ROC) values are obtained using the Equation (5.1). In addition, when observing the SOC behavior shown in Figure 5.3, it can be emphasized that the rate of change of SOC for the power rating above 25 [kW] is very small.

$$ROC = \frac{\Delta f}{\Delta P} \tag{5.1}$$

Where Δf is change in frequency, and ΔP is change in power rating

Table 5.1: The frequency for given power rating measured at 59500s of time

BESS Power rating[KW]	Frequency(at time: 59500s)[Hz]	Rate of change(ROC)
5	50.089	–
10	50.074	-0.003
15	50.064	-0.002
20	50.058	-0.0012
25	50.052	-0.0012
30	50.049	-0.0006
35	50.046	-0.0006

5.2 2nd Scenario: High consumption and low RE

The simulated frequency with a BESS of 5 [kW] power rating is observed to violate the defined limits during the high consumption and low RE scenario. This issues can be mitigated by performing a sensitivity analysis as done in section 5.1. The considered BESS power rating applied in the system are 5, 10, 15, 20, 25, 30 and 35 [kW], and the resulted frequency, active power at BESS ac terminal and SOC are given in Figures 5.4, 5.5 and 5.6 respectively. As expected, it can be seen that the increase in BESS power rating increases the rate of charging and thus more active power is absorbed by BESS during overproduction and then delivered to grid during peak load. As consequence, the frequency deviation is reduced as well. By evaluating the rate of change of frequency and the SOC with respect to BESS power rating, it is obvious that the rate of change is very small for the power rating above 25 [kW].

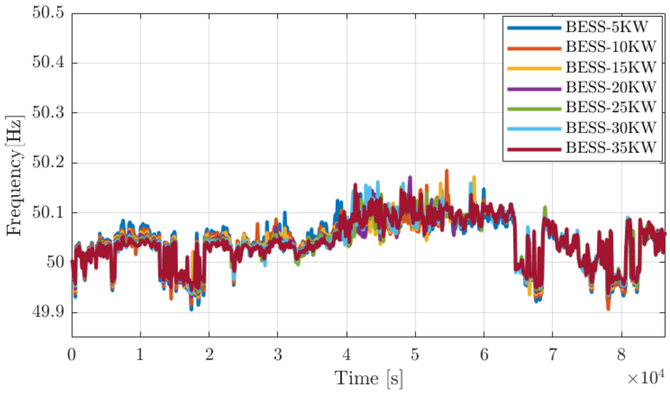

Figure 5.4: Frequency for different BESS power rating

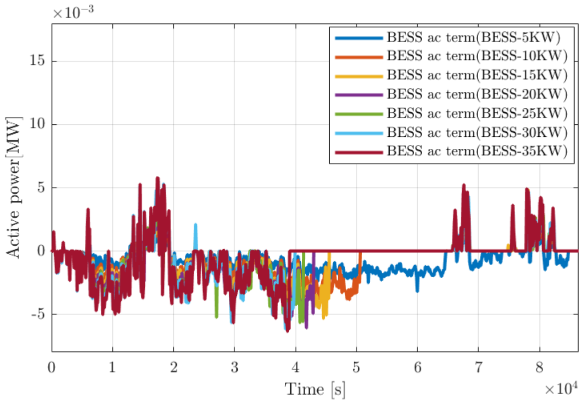

Figure 5.5: Active power at BESS ac terminal

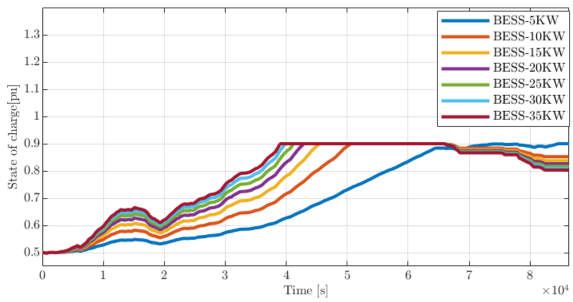

Figure 5.6: State of charge

The main objective of this chapter was to find the proper size for BESS to mitigate the frequency stability issues. To achieve this, the sensitivity analysis is performed by applying 5, 10, 15, 20, 25, 30 and 35 [kW] BESS power rating in both low and high consumption scenario. The resulted frequency and SOC in both scenarios shows that the more the BESS power rating, the further the frequency deviation is reduced. However, the rate of change of frequency and SOC respective to power rating is observed to be very small for the operating rate level above 25 [kW]. Therefore, the power rating level of 25 [kW] is chosen to be the suitable size for BESS in this project.

In the next Chapter, the discussion on overall project work and the obtained results will be provided.

6 Discussion

This chapter discusses about some of the important points, simplifications and assumptions that are made throughout the project, and how they helped to reach the project goal. In addition, the obtained results for different scenarios will be discussed. The project goal was about to develop a BESS control strategy for supporting the frequency stability in a microgrid containing the RESs. The considered energy system model investigated in this project is the Livø islanded microgrid powered by DG, WT and PV. In the process of developing a BESS control, different aspects associated with the battery, frequency control and the used components in power system model were investigated. By analysing the performance and properties of different type of batteries, it is found out that the Li-ion and flow-batteries have a great potential and are good candidates for frequency stability into grid, and this matches the type of battery of Vanadium Redox Flow battery that is used in Livø energy system. However, the battery in this project was modelled as voltage source as Vanadium Redox Flow battery model was not available in PowerFactory. Furthermore, the conventional frequency control methods were examined, and the applied BESS in this project was used o replace the DG primary control on the Livø power system. The developed BESS control is set to be activated when the frequency deviation exceeds 20 [mHz], and with droop control gain of 0.004 [pu] which means that the BESS full power is activated when the frequency deviation is equal or greater than 200 [mHz]. The performance of the developed BESS control strategy was examined using two critical scenarios, and this was carried out through performed simulations in DIgSILENT PowerFactory. The simulated results of system before and after and BESS sizing are to be discussed in the next two sections.

6.1 System operation before BESS sizing

The performance of the developed BESS control integrated in system model is examined using two critical scenarios. In the 1st scenario, the system was operating at low load demand while the RE production was high. After implementing the BESS control strategy as described in 4.1 , the frequency deviation from the maximum allowed limit of dead-band range was observed to decrease from 0.14 [Hz] to 0.09 [Hz] that corresponds to 35.7% of reduction while the deviation from the minimum allowed limit decreased from 0.05 [Hz] to 0.03 [Hz] corresponding to 40% of reduction.

The 2nd scenario was performed during high consumption and low RE as described in section 4.2. As shown in Figure 4.4, with the BESS control, the measured maximum frequency was reduced from 50.17 [Hz] to 50.14 [Hz], this correspond to 20% reduction of frequency deviation, while the minimum frequency was increased from 49.87 [Hz] to 49.91 [Hz] which corresponds to 36.3% reduction of frequency deviation. This is an indication that the developed BESS control strategy is working as expected. However, it is obvious that the frequency deviation needs to be reduced more, and this can be achieve by increasing the BESS power rating as discussed in next section.

6.2 System operation after BESS sizing

The BESS sizing was performed using sensitivity analysis method. This was also done by applying 10, 15, 20, 25, 30 and 35 [kW] BESS rating in the system for both scenarios. According to the simulated results in both 1st and 2nd scenario described in section 5.1 and 5.2, the frequency deviation was observed to decrease with increasing power rating. However the rate of change of frequency with respect to power rating is very small for for rating above 25 [kW] and does not have a significant impact. Therefore, the power rating of 25 [kW] is chosen to be the suitable size of BESS. By applying the 25 [kW] in the 1st scenario, the minimum and maximum frequency are measured to be 49.7 [Hz] and 50.05 [Hz] which gives 80% and 71.4% of reduction of frequency deviation respectively. In the second scenario,with 25 [kW], the minimum and maximum frequency are measured as 49.94 [Hz] and 50.15 [Hz] which correspond to 63.6% and 13.3% reduction of frequency deviation respectively. In this scenario, it is observed that the maximum frequency has not significantly changed because the SOC reached the allowed maximum limit (SOC=0.9) at $4.09 \cdot 10^4$ [s] or $11:30$ as shown in Figure 5.6, and thus the BESS could not absorb more power from the grid during this time. This could be improved by connecting the HP or el-boiler to discharge the BESS power and convert it to heat.

7 | Conclusions

The purpose of this project was to develop a BESS control strategy to support the frequency in the system with RESs. The developed control strategy was implemented in the Livø micrigrid containing the DG, WT and PV. To examine the impact of control strategy on the system model, the two critical scenarios were considered in this project, the first is low consumption & high RE and the second is high consumption & low RE. According to the simulated results, the BESS control with 5 [kW] as described in the 1st scenario helped to reduce the frequency deviation by 40% and 35.7% from lower and upper allowed dea-band limits, respectively. In the second scenario provided in Section 4.2, the BESS control is found to reduce the frequency deviation by 36.3% to 20% from lower and upper allowed dead-band limits respectively. This is the indication that the developed control strategy is able to support the frequency stability as well as increasing the utilization of RESs in grid. Furthermore, the sensitivity analysis was performed to find out a suitable BESS size aiming to reduce more the frequency deviation, and hence keep it within the allowed limits. As described in Chapter 5, the suitable size of BESS is found to be 25[kW], and with this new size has reduced the frequency deviation by 80% and 71.4% from lower and upper dead-band limits, while in second scenario the frequency deviation has been reduced by 63.6% and 13.3%. From this observation, it can be concluded that the BESS control strategy has contributed in frequency stability as expected. However, for future work, it can be suggested to optimize the utilization of flexible load along with the BESS in order to reduce the frequency deviation by 100% in the scenarios, and this can guarantee increase of more RES and more reduction of DG in the system on Livø island. Therefore, the following list of the main points to examine for the future work are following:

- Optimising the BESS control: To maintain the frequency within dead-band limits for both scenarios.
- Optimizing the utilization of flexible loads in the grid. To improve the power management in the system
- Voltage stability: In this project, the investigation of voltage stability was not taken into account. Therefore, it is needed to consider the voltage stability in future to ensure a strong and reliable power system.

Bibliography

[1] A record year: Wind and solar supplied more than half of denmark's electricity in 2020. `https://stateofgreen.com/en/partners/state-of-green/news/a-record-year-wind-and-solar-supplied-more-than-half-of-denmarks-electricity-in-2020/`. Published January 2021.

[2] Future system inertia 2. `https://www.fingrid.fi/globalassets/dokumentit/fi/yhtio/tki-toiminta/raportit/nordic-report-future-system-inertia2_vfinal.pdf`. Published by ENTSO-E AISBL Avenue Cortenbergh 100 Belgium.

[3] Paul Breeze. *Power System Energy Storage Technologies*. Joe Hayton, mariana l. kuhl edition, 2018. ISBN: 978-0-12-812902-9.

[4] David Wenzhong Gao. *Energy Storage for Sustainable Microgrid*. Amsterdam : Academic Press. Elsevier.

[5] Miljø- og Fødevareministeriet Naturstyrelsen. Livø-en bæredygtig ø. pages 7–34, Jun 2020.

[6] Livø. `https://naturstyrelsen.dk/naturoplevelser/naturguider/livoe/`. -.

[7] Magdi S. Mahmoud. *Microgrid: Advanced control methods and renewable energy system integration*. Amsterdam, Netherlands : Butterworth-Heinemann, magdi s. mahmoud edition, 2017. ISBN : 0-08-101262-4 ISBN : 0-08-101753-7.

[8] P. Kundur. *Power System Stability and Control*. McGraw-Hill, Inc.

[9] Advanced Course in Electrical Power System. Lecture02:frequency stability, 2020.

[10] Oriol Gomis-Bellmunt Francisco Diaz-Gonzalez, Andreas Sumoer. *Energy Storage in Power Systems*. John WileySons Ltd.

[11] AECOM Australia Pty Ltd. Energy storage study funding and knowledge sharing priorities, 2015.

[12] William E. Kramer Sudipta Chakraborty, Marcelo G. Simões. *Power Electronics for Renewable and Distributed Energy Systems*. Springer London Heidelberg New York Dordrecht, sudipta chakraborty, marcelo g. simões, william e. kramer edition, 2019. ISSN 1865-3529, ISBN 978-1-4471-5103-6.

[13] Energinet.dk. Technical regulation 3.3.1 for electrical energy storage facilities, 2019.

[14] James R. Bumby Jan Machwski, Janusz W. Bialek. *Power System Dynamics 2nd edition.* John Wiley&Sons, Ltd.

[15] Swp-25 kw. https://www.solid-group.dk/solid-wind-power/moelletyper/swp-25kw/. -.

[16] Get data. http://climatestationdata.byg.dtu.dk/GetData. -.

[17] DIgSILENT PowerFactory. Pv system, technical reference, 2020.

A System model in PowerFactory

The whole system model in PowerFcatory is presented in Figure A.1, the WT & PV are enclosed in green, the Diesel generator (DG) is enclosed in red and the BESS model is enclosed in orange. In addition, the loads are numbered as L1–>L18 plus 2 flexible loads (HP and el-boiler).

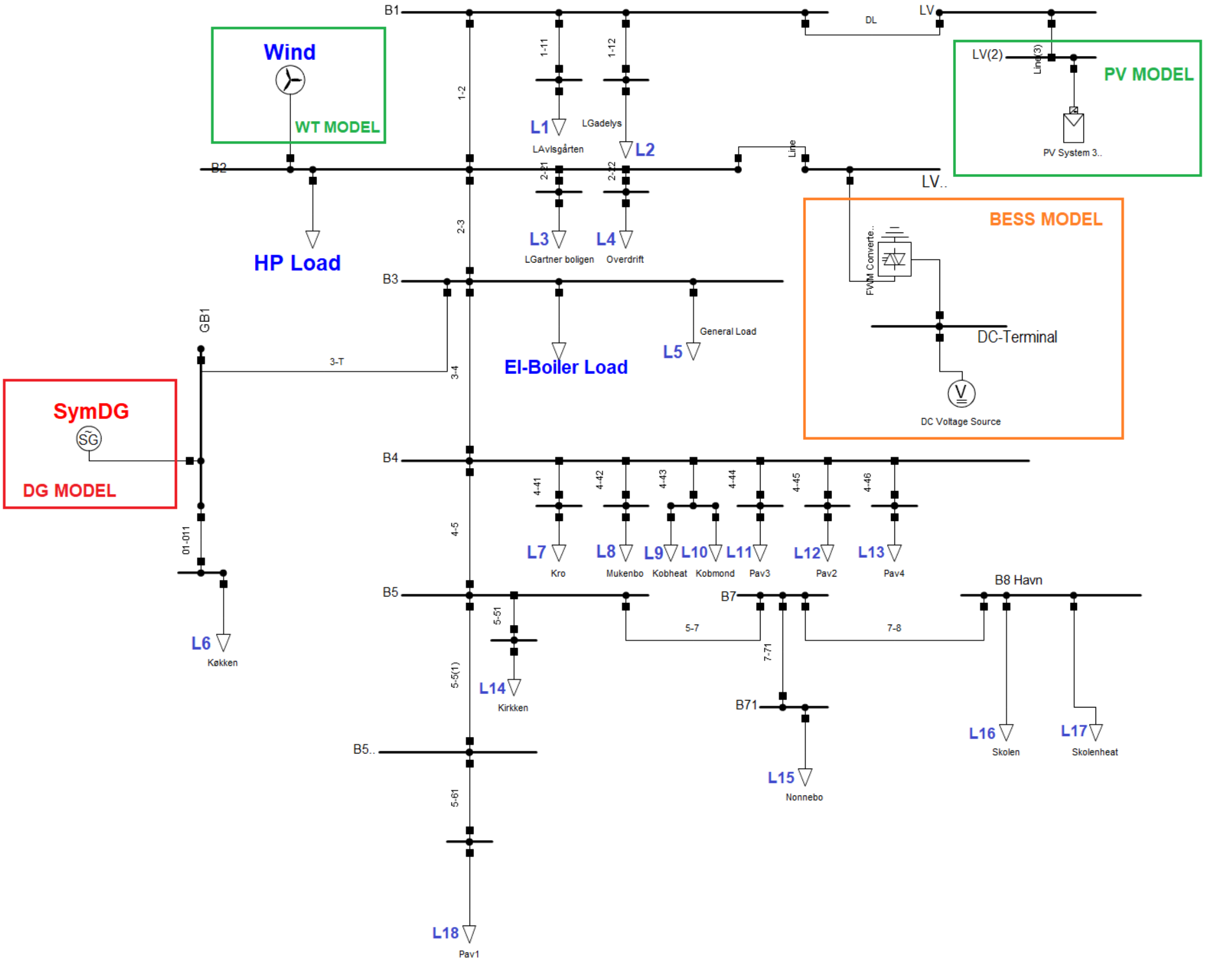

Figure A.1: The whole system model in PowerFactory

A.1 BESS model

The BESS control strategy is developed with the purpose to regulate the system frequency at the normal value in the system containing the RESs. This BESS consists of various elements and controllers as shown in Figure A.2.

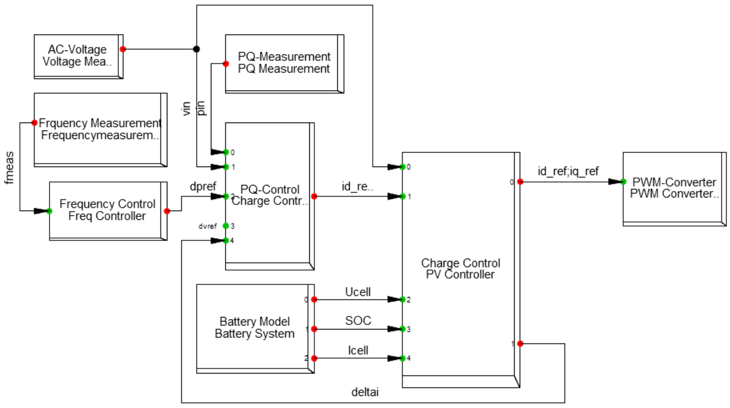

Figure A.2: Schematic diagram of BESS frame

- **PLL**: This is used to track the frequency using the measured input voltage signal in grid.
- **Frequency controller**: This is modelled as shown in Figure A.3, where it starts by comparing the measured frequency from PLL block to the frequency reference set as 1 [pu] equivalent to 50 [Hz]. The output signal leads to deadband block with a gain of 0.004 [pu] identical to 20 mHz. The output information from dband block leads to droop block with a gain of 0.004 [pu] identical to 200 [mHz] of frequency deviation. This means that if the frequency deviation is equal or above 200 [mHz], then the BESS will activate the full power. The offset block compensate the output dpref in case it is not equal to zero.

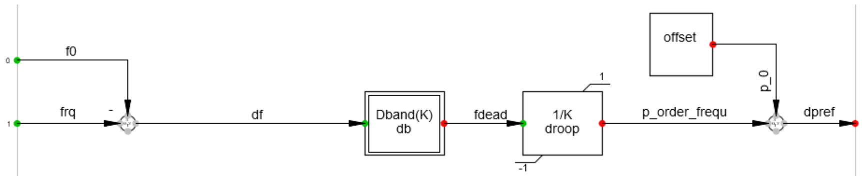

Figure A.3: Schematic for frequency controller model

- **PQ controller**: This controller includes the active power and voltage control as presented in Figure A.4 . For the active power control, the dpref from frequency control is first compared to the measured active power in grid, the output signal is adjusted by PI control block which thereby generate the active current i_{dref}. In addition, the voltage is adjusted by comparing the measured voltage and the voltage reference and then output the reactive current signal i_{qref}.

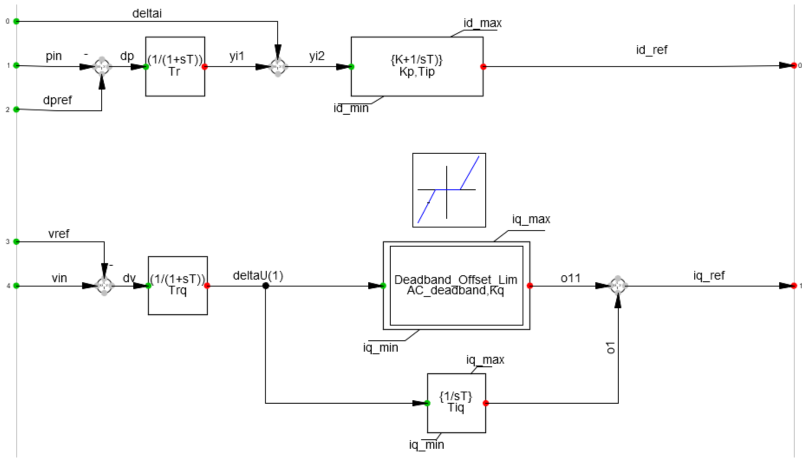

Figure A.4: Schematic for PQ model

Table A.1: PQ controller settings

Parameter	Value
T_r(Filter time constant, active path [s])	0.05
T_{rq}(Filter time constant, reactive path [s])	0.01
K_p(Proportional gain-id-PI-controller [pu])	2
T_{ip}(Integrator time constant -id-PI-contrl [s])	0.1
AC deadband for proportional gain[pu])	0.1
K_q(Proportional gain for AC-volt support [pu])	2
T_{iq}(Integrator time constant iq-I-contrl [a])	1
i_{dmin}(Min discharging current [pu])	-1
i_{qmin}(Min reactive current [pu])	-1
i_{dmax}(Max charging current [pu])	1
i_{qmax}(Max reactive current [pu])	1

- **Charge controller**: This controller receives the output current signals from PQ controller together with the information about the battery state of charge (SOC) from battery model, it decides whether the battery charges or discharges depending on the frequency condition in grid. The schematic for charge controller is given in Figure A.5 and parameter settings in table A.2.

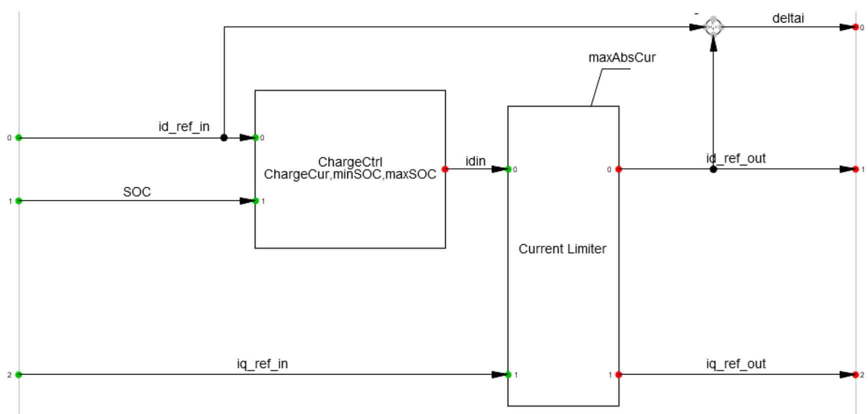

Figure A.5: Charge control model

Table A.2: Charging control

Parameter	Value
Min charging current[pu]	0.8
Min SOC[pu]	0.1
Max SOC[pu]	0.9
Max AbsCur[pu]	1

- **Battery model**: This model is provided with a DC-current signal, and this is processed through different blocks for integrator and gain so as it generates the proper output DC-voltage, the SOC and DC-cell voltage as shown in Figure A.6.

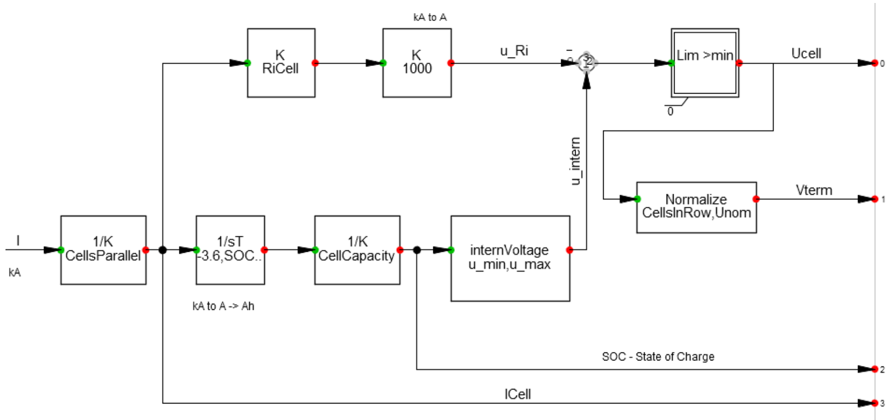

Figure A.6: Battery model

Table A.3: Battery settings

Parameter	Value
SOCo (Initialization) [pu]	0.5
Cell capacity per cell [Ah]	4
V_min(Voltage of empty cell) [V]	12
V_{max} Voltage of full cell [V]	13.85
Parallel cells	12
Cells in series	65
V_{nom} Nominal voltage of source [kV]	0.9
R_i Intern resistance per cell [Ω]	0.001

A.2 PV model

The whole PV system model is shown in Figure A.7. Each block represents either a DSL model or a measurement component.

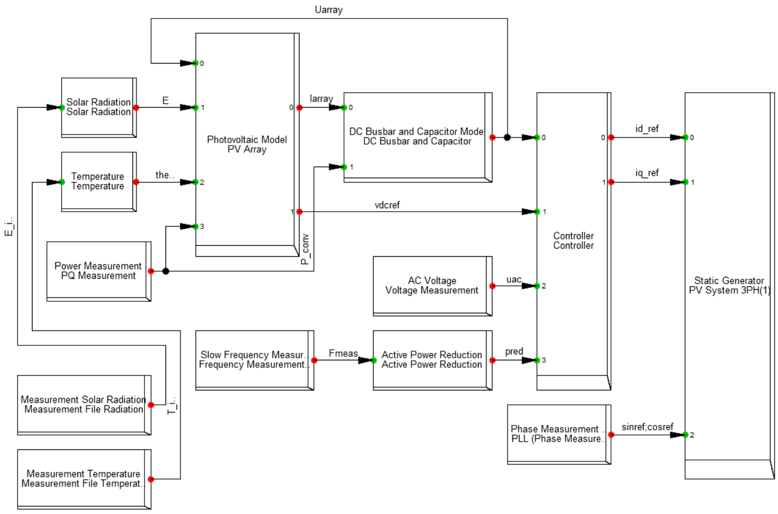

Figure A.7: PV system model frame

- **Photo-voltaic model**: This contains a dsl model for PV model. The used settings in this model are presented in Table A.4.

Table A.4: PV array settings

Parameter	Value
V_O(Open-circuit voltage of module at STC [V])	43.8
V_{MPP}(MPP voltage of module at STC) [V]	35
I_{MPP}(MPP current of module at STC) [A]	4.58
I_{sc} (Short circuit current of module at STC) [A]	5
Temperature correction factor(Voltage) [1/K]	−0.0039
Temperature correction factor(Current) [1/K]	0.0004
Time constant of module [s]	0
n_{series}(Number of modules in series)	20
$n_{parallel}$(Number of modules in parallel)	150

- **Controller**: This controller model is used for voltage and reactive power control. The controller settings can be seen in Table A.5.
- **Measurement solar radiation**: This block contains the imported solar radiation file with radiation profile.
- **Static generator**: This plays a role as an inverter
- **AC voltage**: This is used to measure the ac voltage used to detect the fault
- **PLL**: This is used to calculate the frequency form the measured voltage in grid.
- **PQ measurement**: This measures the active and reactive power in grid, which are needed for control feedback

Table A.5: Controller settings

Parameter	**Value**
K_p(Gain)	0.005
T_{ip}(Integration time constant)[s]	0.03
T_r(Measurement Delay[s]	0.001
T_{mpp} (Time Delay MPP-Tracking)[s]	5
Deadband for dynamic AC voltage support[pu]	0.1
K_{FRT} (Gain for dynamic AC voltage support)	2
id_{min}Minimum active current limit[pu]	0
U_{min}Minimum allowed DC-voltage[V]	200
iq_{min}(Minimum reactive current limit[pu])	-1
id_{max}(Maximum active current limit[pu])	1
iq_{max}(Maximum reactive current limit[pu])	1
maxAbsCur (Maximum allowed absolute current[pu])	1
maxIqMax.abs (reactive current in normal operation)[pu]	1

B | Actual load profile

The various actual load profile for the whole year at Livø can be seen in Figure B.1 for L1-L3, B.2 for L4-L6, B.3 for L7-L9, B.4 for L10-L12, B.5 for L13-L15 and B.6 for L16-L17. From these graphs, the peak load has been observed during Autumn and low consumption during Spring.

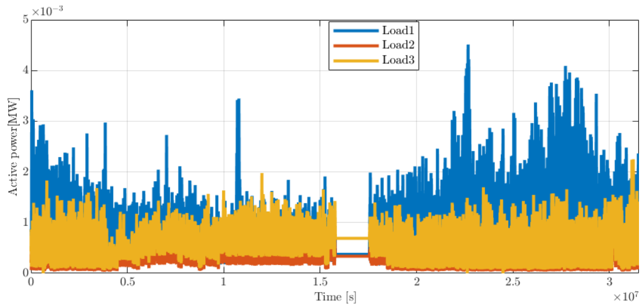

Figure B.1: Load 1-3

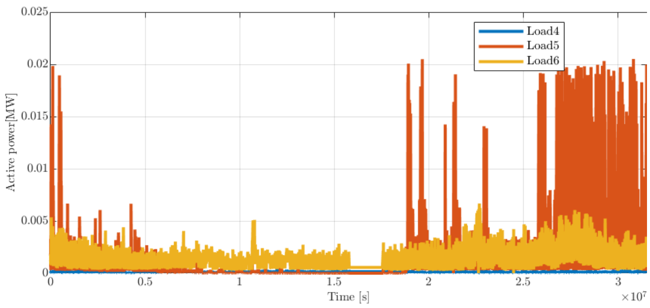

Figure B.2: Load 4-6

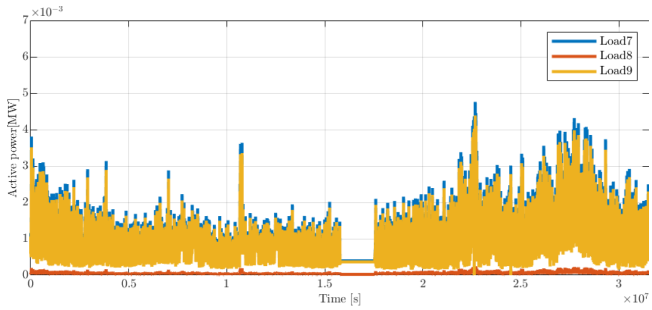

Figure B.3: Load 7-9

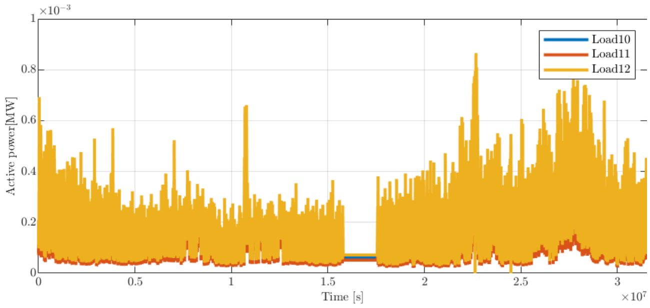

Figure B.4: Load 10-12

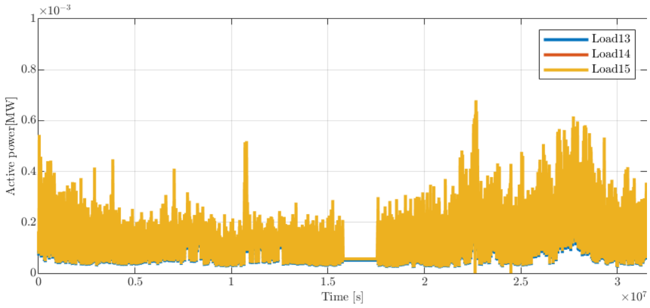

Figure B.5: Load 13-15

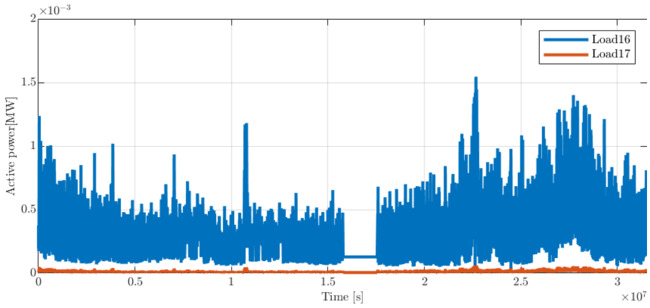

Figure B.6: Load 16-17